International Journal of Coal Geology 319 (2026) 104990

Contents lists available at ScienceDirect

International Journal of Coal Geology

journal homepage: www.elsevier.com/locate/coal

Evaporite minerals from the coal mines of the Czech part of the Upper Silesian Basin, including a new mineral králíkite ($BaCl_2·2H_2O$)

Dalibor Matýsek [a], Jakub Jirásek [b,*], Juraj Majzlan [c], Jan Filip [d], Michal Osovský [e], Jörg Göttlicher [f]

[a] Department of Geological Engineering, Faculty of Mining and Geology, VŠB-Technical University of Ostrava, 17. listopadu 15/2172, 708 00 Ostrava-Poruba, Czech Republic
[b] Department of Geology, Faculty of Science, Palacký University Olomouc, 17. listopadu 1192/11, 771 46 Olomouc, Czech Republic
[c] Department of Geosciences, Friedrich Schiller University Jena, Carl-Zeiss-Promenade 10, 07745 Jena, Germany
[d] Regional Centre of Advanced Technologies and Materials, Czech Advanced Technology and Research Institute, Palacký University Olomouc, Šlechtitelů 27, 783 71 Olomouc, Czech Republic
[e] OKD, Mining plant 1, Čs. armády 1, 735 06 Karviná-Doly, Czech Republic
[f] Institute for Photon Science and Synchrotron Radiation, Karlsruhe Institute of Technology, Hermann-von-Helmholtz-Platz 1, 76344 Eggenstein-Leopoldshafen, Germany

ARTICLE INFO

Keywords:
Evaporite
Coal
New mineral
Králíkite
Halide
Brines

ABSTRACT

The Czech part of the Upper Silesian Basin is still a home of bituminous coal mining in Europe. The underground mines there feature rich assemblages of evaporite minerals that precipitate from the water flowing through the mines. The minerals occur in stalactites, rarely as cave pearls. The predominant mineral of the stalactites is halite (NaCl). The first group consists of halite stalactites with sylvite (KCl), carnallite ($KMgCl_3·6H_2O$), and rare gypsum ($CaSO_4·2H_2O$) and baryte ($BaSO_4$) on their surface. Orange coloration may be caused by lepidocrocite or akageneite (both Fe-oxyhydroxides). In the second group, halite is covered by carnallite, králíkite ($BaCl_2·2H_2O$), and $SrCl_2$ hydrates. In the third group, halite is associated with burkeite [$Na_6(CO_3)(SO_4)_2$], blödite [$Na_2Mg(SO_4)_2·4H_2O$], kainite [$KMg(SO_4)Cl·3H_2O$], thénardite (Na_2SO_4), and trona [$Na_3H(CO_3)_2·2H_2O$]. Some of the stalactites are dominated by sulfates, with starkeyite, hexahydrite, epsomite (all representing $MgSO_4$ hydrates), or thénardite. The fourth group comprised a single sample, a stalactite with α-calcium formate and králíkite. All these minerals precipitate from brines that acquire their dissolved load primarily from Early Badenian groundwater bodies, frequently in direct contact with the Carboniferous basement rocks. These are fossil marine waters with total mineralization >10 $g·l^{-1}$, rich in NaCl, locally also in CH_4 and CO_2, and enriched in Sr^{2+}, Ba^{2+}, I^- and Br^-. These types of water also led to precipitation of the newly described mineral králíkite. Owing to the low solubility of baryte, králíkite can only form from water strongly depleted in sulfate. The brines are locally mixed with sulfate-rich acid mine drainage water, resulting in some sulfate-rich compositions observed in this work. Our study highlights some processes tightly linked to coal and coal mining, namely formation of secondary mineralization underground and its possible environmental impact during and after the mining. As the coal mines are being successively shut down, this aspect should be prominent for the middle- to long-term elimination of hazards related to recent and current coal mining.

1. Introduction

Coal is a complex geomaterial which contains predominantly organic matter, but also water, gaseous substances, and minerals. The mineral content plays crucial role in amount of the volatile matter and ash left after coal burning (Thomas, 2013). In some cases, metals were recovered from coal or coal ash on an industrial level (e.g., uranium: U.S.A. - U.S. Energy Information Agency, 2011, Czechoslovakia – Aulický et al., 2003; germanium: China, Russia - Sverdrup and Haraldsson, 2024). Some of the coal minerals seem to carry a valuable resource for the future, such as uranium (Jedrzejek et al., 2025), germanium (Dai et al., 2014; Dedovets, 2025), lithium (Zhao et al., 2019; Wei et al.,

* Corresponding author.
E-mail addresses: dalibor.matysek@vsb.cz (D. Matýsek), jakub.jirasek@upol.cz (J. Jirásek), juraj.majzlan@uni-jena.de (J. Majzlan), jan.filip@upol.cz (J. Filip), joerg.goettlicher@kit.edu (J. Göttlicher).

https://doi.org/10.1016/j.coal.2026.104990
Received 9 January 2026; Received in revised form 13 March 2026; Accepted 13 March 2026
Available online 14 March 2026

2020), rare earth elements (Dai et al., 2016a, 2016b), niobium (Dai et al., 2016b) and others. On the other hand, there may be some potential risks connected with the coal mineralization as well. Potentially harmful or toxic chemical elements present in the coal minerals may be released during coal washing, coking, burning, storage of ash, as well as coal weathering in the mines (e.g., Wagner and Hlatshwayo, 2005; Bartoňová et al., 2020; Wei and Song, 2020; Hu et al., 2022; Wang et al., 2024; Wei et al., 2024). Considering the scientific aspects, minerals in coal may be useful for establishing the paleoenvironmental conditions in the coal swamps, as well as the post-depositional geological processes (Vassilev et al., 2010a, 2010b; Thomas, 2013; Finkelman et al., 2019). For these reasons, and with the support of new techniques of mineralogical research, coal mineralization has been studied in previous decades across many sedimentary basins of the world.

Some of coal mineralization is primary (e.g., quartz, clay minerals, carbonates), representing particulate matter transported into the coal swamp. However, most of the minerals recognized from coal are products of later processes, such as diagenesis, hydrothermal alteration, or other late modifications (see Finkelman et al., 2019, for details). Our study is dealing with uncommon and poorly studied minerals that originate from salt brines. There are similar mineralizations known from several coal occurrences, e.g., Bobov Dol, Bulgaria (halite, sylvite - Vassilev et al., 1994), Sozopol Bay, Bulgaria (halite - Yossifova et al., 2011), Qiangtang Basin, China (halite, anhydrite – Fu et al., 2013), Ruhr District, Germany (halite, gypsum (Grobe and Machel, 2002; Tran et al., 2020), Pera-Lakkos, Greece (halite, sylvite - Kalaitzidis et al., 2010), Acıgöl Basin, Turkey (halite, gypsum – Karayiğit et al., 2015), and Karapınar-Ayrancı, Turkey (halite, gypsum, bassanite - Oskay et al., 2016).

Our study focused on the Czech part of the Upper Silesian Basin (hereinafter CUSB), one of very few locations of remaining bituminous coal mining in Europe (Sivek et al., 2020). The territory hosts the last active underground mine, which will probably cease production in early 2026 due to the high operation costs, as well as the European efforts towards green energy transition (e.g., Apostu et al., 2022; Elavarasan et al., 2022; Filipović et al., 2022). During the coal extraction, the mineralogical studies were to a great extent limited by complicated access to the mines and quickly advancing workplaces, usually not allowing to preserve any interesting geological sites. However, after the mine closure, the new geological and mineralogical material will become completely inaccessible, with an exception of a few samples stored in archives and museums. Therefore, in the last decade, we focused on rescue research of some interesting mineralizations related to the salt brines that flow into the coal mines. The results, which include some minerals new for coal, rare worldwide, and one new mineral (approved by the International Mineralogical Association, Commission on New Minerals and Mineral Names), are presented in this article.

2. Geological settings and previous studies

The Upper Silesian Basin is among the last bituminous coal basins with active mining in Europe. It is the most important of these basins in terms of its recent production (Starý et al., 2024; Malon and Tymiński, 2025).

The Upper Silesian Basin is an erosional relic of an originally larger structure, with roughly triangular shape and a present area of ca. 7000 km^2. Most of it belongs to Poland, while the Czech part covers ca. 1550 km^2 - Fig. 1 (Dopita et al., 1997). The basin is situated within the the basin belt stretching in the eastern tropical Pangea, affected by the Variscan Orogeny. The basin represents the final evolutional stage of the larger Moravo-Silesian Basin (Kalvoda et al., 2008) which opened during the early Devonian as a shallow marine basin and turned into a deep marine synorogenic basin during the Tournaisian and Viséan (Kalvoda et al., 2008). The basin sedimentation became terrigenous during the Serpukhovian with presence of coal swamps and frequent marine ingressions (Jirásek et al., 2018). Following a sedimentation hiatus, the early Pennsylvanian sediments were purely continental, with significant amounts of peat as a precursor of economic coal seams (Opluštil et al., 2022). The sedimentary record in the CUSB ends with Bashkirian units due to later erosion, while in the neighbouring Polish territory, it continues into the early Kasimovian (Laurin et al., 2024).

Table 1
Locations of the CUSB mines dumps mentioned in the text. Arranged in alphabetical order.

Mine	Municipality	GPS coordinates	No. in Fig. 1
9. květen (also Suchá - Stonava)	Stonava	N 49° 48.013′ E 018° 30.190’	1
Barbora (also 1. máj)	Karviná-Doly	N 49° 49.366′ E 018° 28.446’	2
Čs. pionýr	Petřvald	N 49° 50.525′ E 018° 24.130’	3
ČSA – Jan Karel	Karviná-Doly	N 49° 50.745′ E 018° 29.786’	4
ČSA – Jindřich	Karviná-Doly	N 49° 50.354′ E 018° 28.025’	5
ČSM	Stonava	N 49° 49.063′ E 018° 32.910’	6
Dukla	Havířov-Dolní Suchá	N 49° 48.652′ E 018° 26.515’	7
Hlubina (Ostrava)	Ostrava-Moravská Ostrava	N 49° 49.270′ E 018° 16.685’	8
Jeremenko	Ostrava-Vítkovice	N 49° 48.308′ E 018° 16.220’	9
Ludvík	Ostrava-Radvanice	N 49° 48.565′ E 018° 21.445’	10
Lazy	Orlová-Lazy	N 49° 49.783′ E 018° 26.678’	11
Petr Bezruč	Ostrava-Slezská Ostrava	N 49° 50.528′ E 018° 18.474’	12
Rudý říjen	Ostrava-Heřmanice	N 49° 51.824′ E 018° 18.957’	13
Šalamoun	Ostrava-Moravská Ostrava	N 49° 49.879′ E 018° 16.769’	14

The Serpukhovian paralic Ostrava Formation within the Czech part (Fig. 1b) contains up to 170 coal seams with an average thickness of 0.73 m, while the Bashkirian continental Karviná Formation (Fig. 1b) hosts up to 90 coal seams with an average thickness of 1.80 m. The lithology of the coal-bearing sequences is rather simple: it is dominated by sandstones over siltstones, while claystones and conglomerates are less important (Havlena, 1982; Dopita and Kumpera, 1993). Dozens of underground mines were operating during the 20th century in an area of ca. 400 km^2 aiming for both Serpukhovian and Bashkirian coals, with the peak production of of bituminous coal reaching 25 million tons in 1979 (Dopita et al., 1997).

Hydrogeological conditions of the CUSB are under significant influence of coal mining. The most important natural sources of mine waters are (from the surface down): 1) Quaternary groundwater bodies, 2) Early Badenian groundwater bodies, frequently in a direct contact with the Carboniferous rock massif, 3) fissure system waters of the Carboniferous rock mantle, 4) primary waters bound to tectonic zones of the Upper Carboniferous and the underlying rocks. For the purpose of this study, we must emphasize the reservoir number 2, where confined aquifers reach thickness up to 268 m and pressure up to 10 MPa. From a geochemical point of view, these are fossil marine waters with total mineralization >10 g·l^{-1}, rich in NaCl, locally also in CH_4 and CO_2. They are enriched in Sr^{2+}, Ba^{2+}, I^- and Br^-, and generally have very low $(SO_4)^{2-}$ content. They were responsible for the water bursts in mine workings, as well as for the evaporite mineralization described in this work (Dopita and Kumpera, 1993; Grmela, 1997; Labus, 2005; Dvorský et al., 2007).

The so-called Variegated Beds, stretching across several lithostratigraphic units, are also partly connected to the mineralization described later. These are epigenetically altered segments and bodies of coal-

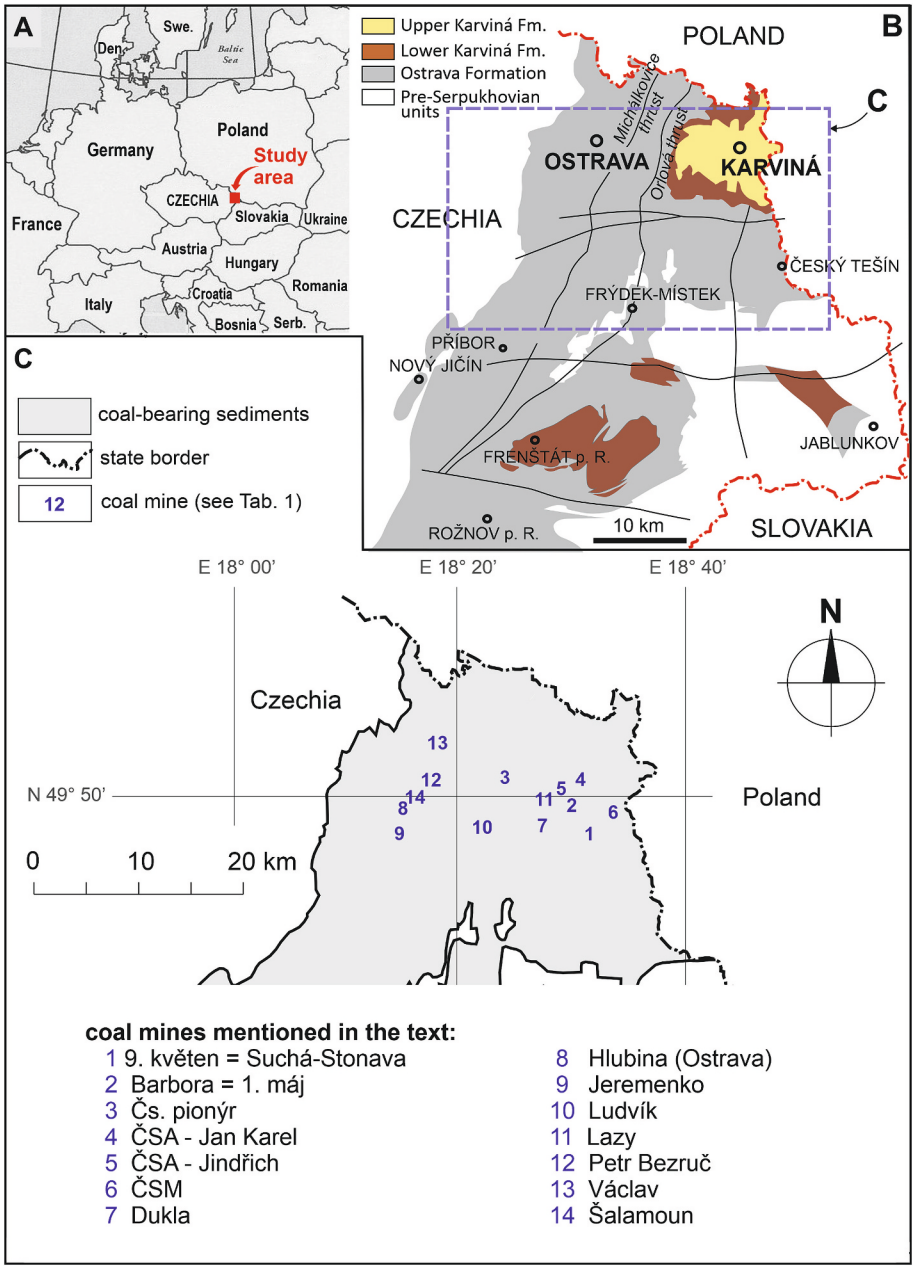

Fig. 1. Generalized map showing: A) the position of the studied area within the Central Europe, B) the geology of the Czech part of the Upper Silesian Basin (according to Opluštil et al., 2022), and c) the location of the dumps mentioned in the text. Their GPS locations are given in Table 1.

bearing sediments. The alteration includes color change of sediments, as well as deterioration in the technological parameters of the coal. Some sulfates (alunite, anhydrite, gypsum, thénardite) were reported from such bodies (Králík, 1980; Klika, 1999; Klika and Osovský, 1999).

The occurrence of salt stalactites has long been known from mine workings in the studied area. The oldest description of halite was mentioned by Kučera (1926) from the Šalamoun Mine in Ostrava, with more details on this sample given by Jaroš (1927). New localities were P. Bezruč and Ludvík mines (Kruťa, 1951). Due to the post-WWII boom of coal mining, five new halite localities were discovered across the whole Czech part of the Upper Silesian Basin (summarized by Kruťa, 1973). Carbonate precipitates from the mine waters were noticed by some authors, e.g. (Maštalíř, 1926–1928; Kruťa, 1951). Due to its presuposed mineralogical uniformity and zero economic value, the interest for such common evaporite mineralization in coal mines was lost and new sites were mostly not published. The most recent work of Matýsek et al. (2014) was dealing with the origin of sulfates in the mines. They are also connected to the infiltration of salt brines and generation of acid mine drainage mineral association, but the article excluded most of the halides.

3. Material and methods

The samples from the ČSA - Jan Karel, Lazy, and ČSM mines were collected by the authors. We also examined significant part of the halite stalactites from the mineralogical collections of Ostrava Muzeum in Ostrava, Moravian Muzeum in Brno, and Prof. Pošepný's Geological Pavilion of the VŠB-Technical University of Ostrava.

Microscopic investigations and SEM-EDS microanalysis were conducted on a FEI Quanta 650 FEG scanning electron microscope (SEM). The analyses were made on natural fracture surfaces without coating under the following conditions: 15 kV beam voltage, 8–10 nA current,

5–6 μm beam diameter, and a vacuum of $<10^{-3}$ Pa. The identification and quantification of spectral lines was performed using the decomposition method employing holographic peak deconvolution. Photomicrographs were obtained with a backscattered electron (BSE) detector in chemical gradient mode.

For most of the described minerals with an exception of králíkite, more reliable wavelength-dispersive spectroscopic (WDS) microanalyses could not be performed due to several reasons: 1) thin sections of chloride and sulfate phases are difficult to prepare because the halite matrix, as well as the investigated minerals themselves, are soft, water soluble, commonly porous, and most of them occur only on their top surface of halite as micrometer-sized crystals; and 2) WDS takes longer than EDS, needs high vacuum and higher beam voltage and current, which result in beam damage caused by mineral dehydration. In fact, many investigated mineral phases are so sensitive that their evaporation was observed even during the EDS analysis.

Powder X-ray diffraction (PXRD) data of králíkite were collected with a Bruker D8 ADVANCE with DAVINCI design (Friedrich Schiller University Jena), and with CuKα radiation, Ni filter, and with a Lynxeye 1D detector. A step size of 0.02° 2θ and the total measurement time was 48 h. Lattice parameters were refined using the program GSAS (Larson and Von Dreele, 2004). The PXRD analyses of other investigated minerals was carried out using a Bruker-AXS D8 Advance (VŠB-Technical University in Ostrava) instrument with a 2θ/θ measurement geometry and the positionally sensitive detector LynxEye under the following conditions: radiation CuKα/Ni filter, 40 kV current, 40 mA voltage, step mode with a step of 0.014° 2θ, a time 0.25 s per step, and a summation of five measurements. The qualitative analysis of diffraction patterns was performed using the EVA software (Bruker-AXS) and the database PDF-2, release 2011 (International Centre for Diffraction Data). The Rietveld method using the TOPAS software, version 5 (Bruker) was applied to verify the analyses and compute the unit cell parameters of mineral phases.

Microchemical analyses of králíkite were performed using wavelength dispersive X-ray spectroscopy (WDS) with an electron microprobe (CAMECA SX100, analyst R. Škoda) at the Laboratory of Electron Microscopy and Microanalysis of the Faculty of Science at Masaryk University in Brno. The standards used were baryte (Ba*L*α), albite (Na*K*α), sanidine (K*K*α), wollastonite (Ca*K*α), $SrSO_4$ (Sr*L*α), hematite (Fe*K*α), NaCl (Cl*K*α), and $PbBr_2$ (Br*L*α). The measurement conditions were: acceleration voltage 15 kV, beam current 4 nA, beam diameter 8 μm.

The micro-X-ray diffraction (μ-XRD) and micro-X-ray fluorescence (μ-XRF) data were collected at the beamline of the Synchrotron Radiation Laboratory for Environmental Studies (SUL-X) at the synchrotron radiation source of the KIT, Karlsruhe, Germany. A silicon (111) crystal pair with a fixed beam exit was used as a monochromator. The X-ray beam was aligned to an intermediate focus and then collimated by slits located at the distance of the intermediate focus to about 100 × 100 μm and subsequently focused with a Kirkpatrick-Baez mirror pair to about 50 × 50 μm at the sample position.

Surface of the samples was mapped with μ–XRF to identify spots with a significant Ba signal. At these spots, μ-XRD analyses were carried out. The μ-XRD data were acquired in transmission mode with a Photonic Science CCD detector XDI VHR-2150. For our experiments, the beamline was operated at a constant energy of 14 keV (λ = 0.886 Å). Powdered LaB_6 was used as the calibrant to verify the wavelength and to refine the sample-to-detector distance. The images were integrated with the program Fit2D (Hammersley, 2016), and the 1D XRD patterns were further used for a full-profile refinement with the program Topas (Bruker).

To ensure congruence of the natural králíkite and its synthetic ($BaCl_2{\cdot}2H_2O$) counterpart, the photoemission spectral characteristics were determined by X-ray photoelectron spectroscopy (XPS) using a PHI 5000 VersaProbe II (Physical Electronics) spectrometer with a monochromatic AlK_α source (15 kV, 50 W and photon energy of 1486.7 eV). The spectra were measured in the vacuum of 1.1×10^{-7} Pa at the temperature of 21 °C. High resolution Ba3d5 and Cl2p spectra were acquired by setting the pass energy to 23.500 eV and the step size to 0.200 eV. For all measurements was used dual beam charge compensation. The XPS spectra were evaluated using the MultiPak (Ulvac - PHI, Inc.) software. All binding energy (BE) values were referenced to the adventitious C1s peak at 284.80 eV.

4. Results

For the purpose of clarity, this section is divided into 1) description of evaporite associations, 2) description of individual minerals, and 3) a part devoted to the description of new mineral králíkite. The ideal formulae are given in Section 4.2.

4.1. Description of evaporite associations

Halite stalactites can be divided into four groups based on their composition. The basis of all salt stalactites is coarse crystalline halite.

The **first group** comprises samples composed of almost pure halite which forms stalactites with more or less prominent skeletal development of cubic crystal aggregates (Fig. 2a, b) on their outer and inner surfaces. These are monomineral, with only rare microscopic baryte or its strontium-rich variety on the stalactite surface (Fig. 2c, d). Exceptionally, microscopic crystals of sylvite up to 60 μm (usually <10 μm) in size (Fig. 2e, f), gypsum crystals, and, even more rarely, carnallite have also been found on the surfaces of the stalactites. Carnallite forms euhedral to subhedral tabular crystals growing on the outer surfaces of halite straws. It was identified in first three types of halite stalactites. The occurrence of bischofite, which sometimes accompanies carnallite on the surfaces of stalactites, might be a product of secondary hydration during the sample storage. These stalactites most likely originated from mixed waters, or waters with significant sulfate content. Typically, this type of stalactite was observed on the shaft supports of the ČSA South and Dukla mines, but are known from the museum samples from other places (Barbora, Čs. pionýr, Suchá-Stonava mines) as well.

According to PXRD, the uncommon orange to red-colored stalactites of the first group (Rudý říjen and Suchá-Stonava mines) contain lepidocrocite and akaganeite, usually in equal proportions. In SEM-EDS, both minerals are difficult to distinguish, forming aggregates of very thin coatings (Fig. 3a) and flaky crystals (Fig. 3b).

The **second group** is represented by stalactites with a more varied composition of microscopic phases on the surface or even in the central channels. In cases, columnar and octahedral halite habitus was noticed (Fig. 3c, d). Carnallite (Fig. 3e) and králíkite were found in relatively large quantities on halite stalactite surfaces. Such material came from the museum samples located at the Hlubina Mine. Only rarely and at only two locations (ČSA Mine – Jan Karel Shaft, and ČSA – Jindřich Shaft), there were microscopic crystals of apparently two different $SrCl_2$ hydrates (Fig. 3f) and several other unidentified phases ($MgCl_2$ hydrate, Na–Ca sulfate chloride).

The **third group** is represented by stalactites and salt crusts from the Lazy site and single museum sample from the Suchá–Stonava Mine, which have a very diverse composition.

The halite straws (elongated hollow cylindrical tubes) at the Lazy site were beige in color and had a bumpy surface. It is likely that the mineralization originated from an highly concentrated solution and that the surface bumps represent the remains of trapped gas bubbles. The base material of the straws is halite. Well-defined growth zones can be observed on the fracture surfaces, separated by other phases and cavities. The surface bumps, approximately 3–5 mm in size, are hollow and contain microcrystalline mineralization composed of water-soluble phases. Powder XRD identified burkeite, blödite, kainite, thénardite, and trona in these cavities. Thermonatrite was identified only tentatively. Blödite (Fig. 4a) was found more commonly in flat crusts formed by dripping of water on the mine base surface. Blödite locally predominates over halite and is glassy, white to very light greenish in color.

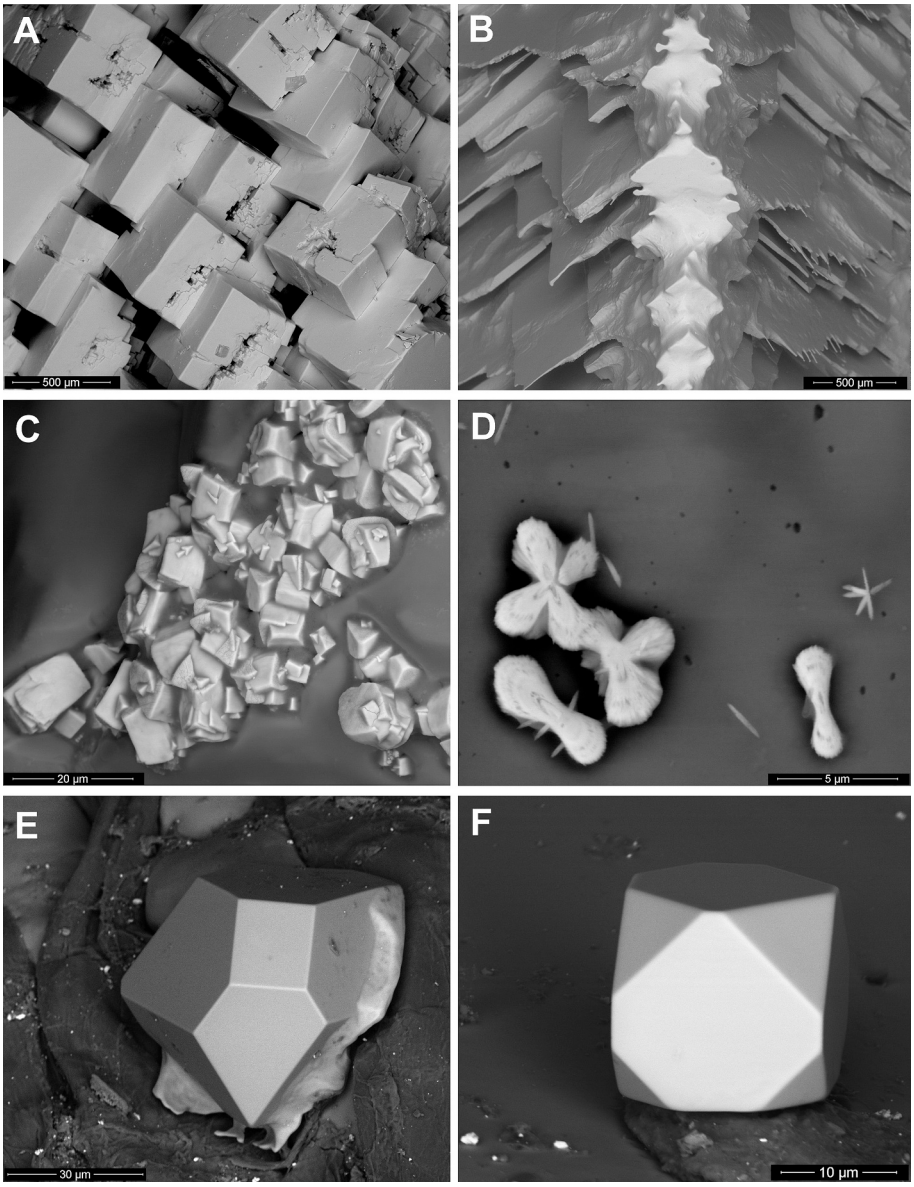

Fig. 2. Back-scattered electron images of group I and II halite stalactite minerals. A – cubic halite crystal with partial skeletal development, ČSA mine, crosscut 11,006; B – skeletal development of halite crystal, ČSA mine, crosscut 11,006; C – aggregate of tabular Sr-rich baryte, ČSA Mine, Jan Karel Shaft; D – Sr-rich acicular baryte bow-ties, ČSA Mine, Jindřich Shaft; E, F – euhedral cubooctahedral sylvite crystals, 1. máj Mine.

A separate type of mineralization was found in small crusts and stalactites at the edges of the mineralized zone. Some of the stalactites were formed by dominant magnesium sulfates (starkeyite - Fig. 4b, with admixtures of hexahydrite, epsomite, and questionable pentahydrite) as well as stalactites dominated by thénardite.

Other phases were found in accessory amounts on the surfaces of beige-colored halite straws: kainite (Fig. 4b), konyaite (Fig. 4c), sylvite, bromine- and exceptionally also iodine-rich sylvite (Fig. 4d), as well as KBr (Fig. 4e) and the tentatively identified syngenite (Fig. 4f) and thermonatrite. Bromine-rich sylvite to KBr, often with an admixture of iodine, formed very thin coatings up to 25 µm in size and only about 1–2 µm thick on the surfaces of the straws. These coatings consist of individual cubic crystals of micrometer size (Fig. 4e). Hydroglauberite (Fig. 5a) with a small admixture of glauberite and traces of bassanite mixed with gypsum were found in the reaction zone between the salt mineralization and the coal seam. The newly described mineral králíkite has been found quite abundantly on the surfaces of stalactites, but it occurs only in locations where the water does not contain dissolved sulfate.

Králíkite is not observable on the surfaces of stalactites either macroscopically or using optical microscopy due to its transparency, irregular distribution, other present mineral phases, and uneven stalactite surfaces. The only way to verify its presence is by SEM using back-scattered electron imaging. It forms thin tabular crystals, usually imperfectly bounded, up to 25 µm long and only 3–5 µm thick, growing parallel to the surface of halite straws, more rarely also in central channels. Details of its identification are given in Section 4.3.

An exceptional sulfate mineralization was detected on the surface of a halite stalactite from the sample No. 97090 (Prof. Pošepný's Geological Pavilion, Suchá–Stonava Mine). In this sample, magnesium sulfate of unknown hydration state and gypsum accompany omongwaite. The latter mineral forms elongated needles with pseudohexagonal shape and length up to 50 µm (Fig. 5e). Unfortunately, there are no available details linked with the geological situation of this specific sample.

The **fourth group** is formed by a single halite museum sample with unique mineralization. The sample is stored in the Moravian Museum in

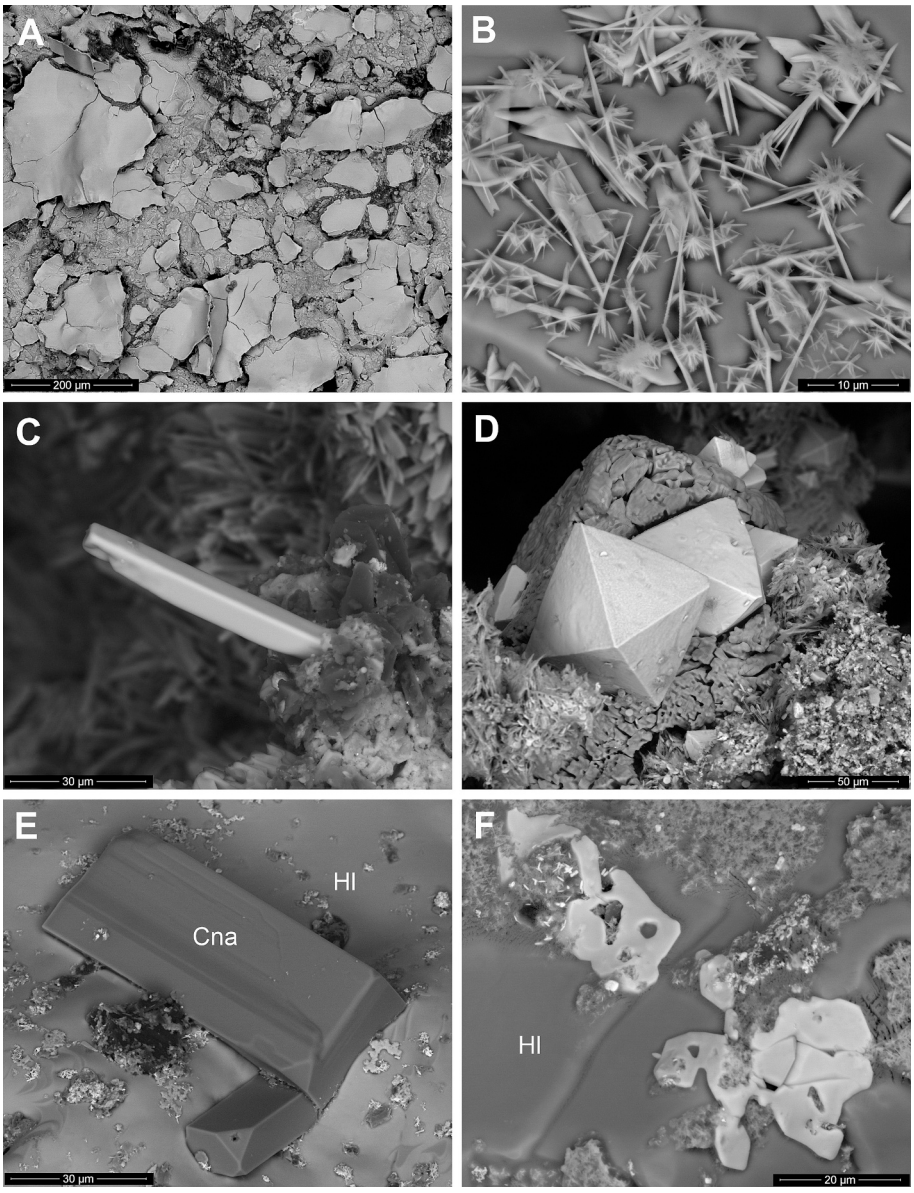

Fig. 3. Back-scattered electron images of group I and II halite stalactite minerals. A – thin coating of teared up Fe-oxides; B – acicular aggregate of unspecified Fe-oxide; C – columnar halite; D – octaheral halite crystals on magnesium sulfate; E – thick tabular crystals of carnallite (Cna) on halite (Hl); F – $SrCl_2$ with uncertain hydratation state (whitish) on halite (Hl). A, C, D: ČSA Mine, Jindřich Shaft, B, E, F: ČSA Mine, Jan Karel Shaft.

Brno (sample Nos. a885–a892, Hlubina Mine). It is a halite stalactite with α-calcium formate and králíkite on its surface. Calcium formate was identified using powder XRD and EDX analysis. It forms pure white tuft-like (Fig. 5f) to kidney-shaped aggregates consisting of microscopic acicular crystals on a fragment of a halite stalactite. The PXRD data correspond well to the orthorhombic modification of calcium formate. The measured lattice parameters were: a = 13.4349(3), b = 10.1825(3) and c = 6.2877(2) Å and are slightly larger than those reported by Watanabé and Matsui (1978): a = 13.407, b = 10.192, c = 6.282 Å. Qualitative EDX microanalysis confirmed the main elements Ca, C, O and minor impurities of Na and Cl. Abundant králíkite was also found on the surface of the studied stalactite. Unfortunately, nothing more is known about the history and detailed origin of the sample.

Carbonate stalactites were noticed only in museum samples. The one from Jeremenko Mine is composed of a mixture of calcite and aragonite with minor monohydrocalcite and halite (Ostrava Museum sample No. M398). Its surface is covered by well developed calcite rhombic crystals. The cave pearls from the Šverma Mine (Ostrava Museum sample No. M2890) are composed of radially-arranged columnar aragonite with botryoidal surface, sometimes forming long prismatic crystals in open spaces.

4.2. *Description of the individual evaporite minerals*

Unit-cell data of all phases identified by powder X-ray diffraction (PXRD) are given in the Electronic Supplementary Material Tables S1 to S22.

4.2.1. *Phases identified with confidence*

α-CALCIUM FORMATE $Ca(HCOO)_2$ – was detected together with králíkite on the surface of a stalactite on a sample from the collection of the Moravian Museum in Brno, forming white irregular aggregates (Fig. 5f) composed of thin tabular on the surface of halite stallactite. It was verified by qualitative SEM-EDS microanalysis and powder X-ray diffraction.

AKAGANEITE $(Fe^{3+},Ni^{2+})_8(OH,O)_{16}Cl_{1.25}{\cdot}nH_2O$ – is, together with

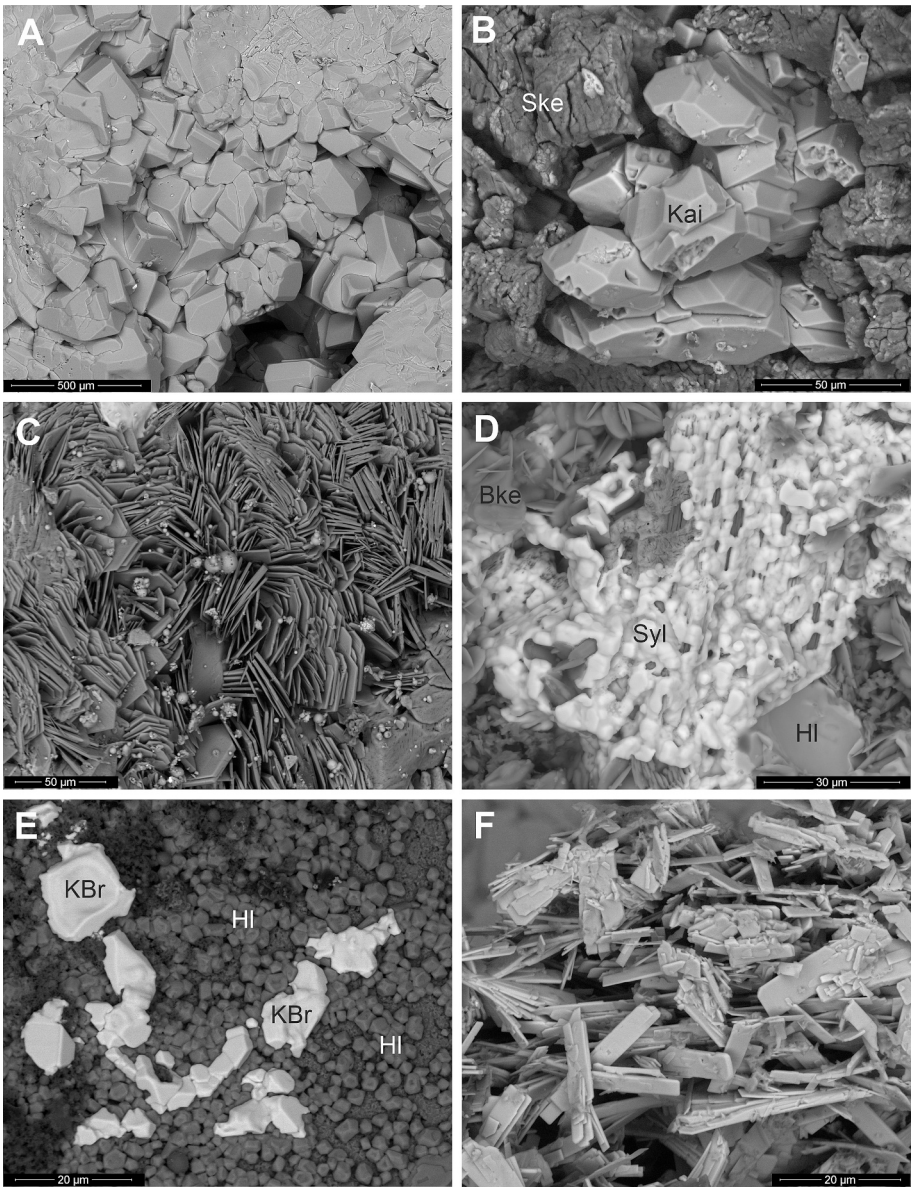

Fig. 4. Back-scattered electron images of group III halite and sulfate stalactite minerals from the Lazy Mine. A – crystal structure of blödite stalactite; B – tabular kainite (Kai) aggregate on starkeyite (Ske); C – druse of thin tabular konyaite; D – Br-rich sylvite (Syl) on halite (Hl) accompanied by burkeyite (Bke); E – KBr showing partial cubic crystal faces on halite (Hl); F – thin tabular crystals of syngenite.

lepidocrocite, a component of the surfaces of orange-colored halite stalactites (Fig. 3a, b) according to powder X-ray diffraction. Supporting data for its confirmation were obtained by SEM-EDS, showing a nickel-free variety.

ARAGONITE $CaCO_3$ – is a major component of precipitation crusts and cave pearls from the Šverma Mine. It has been verified by powder X-ray diffraction analysis.

BARYTE $BaSO_4$ – microscopic baryte and sometimes its strontium-rich variety is commonly present on the surfaces of halite straws, which are formed by crystallization from waters rich in dissolved sulfate. These are tabular (Fig. 2c) or needle-shaped (Fig. 2d) crystals, mostly up to 5 µm in size. The so-called radiobaryte (radium-bearing baryte, see Ulrych et al., 2007; Řanda et al., 2010) is present as a dominant component of crusts that form in pipes that drain water from mines (e.g. Jirásek et al., 2020). These crusts have the appearance of macroscopically homogeneous, beige coatings, but microscopically are formed by tabular crystals of a maximum of 20 µm in size. They are in fact not a product of evaporation, but rather of mixing of mine waters with different chemical composition. The same baryte was recorded from the discharge waters in the Polish part of the Upper Silesian Basin (e.g. Courbet et al., 2016; Wysocka et al., 2019).

BASSANITE $Ca(SO_4)\cdot 0.5H_2O$ – was detected by PXRD as an admixture in a hydroglauberite-impregnated coal sample.

BISCHOFITE $MgCl_2\cdot 6H_2O$ – accompanies carnallite on the surfaces of halite stalactites. Its genesis is probably linked with hydration of carnallite during the storage. Determination only by SEM-EDS microanalyses.

BLÖDITE $Na_2Mg(SO_4)_2\cdot 4H_2O$ – is the dominant component of mineral crusts from the Lazy Mine, formed mostly by imperfectly developed crystals (Fig. 4a). It is white to very light greenish. It has been verified by both SEM-EDS and PXRD.

BURKEITE $Na_6(CO_3)(SO_4)_2$ – was found in the cavities of stalactites from the Lazy Mine. The cavities are filled with a powdery, light beige mass. Burkeite in this mass forms microscopic spherical aggregates, resulting from the oriented growth of tabular crystals (Fig. 5d). It was verified by both SEM-EDS and PXRD.

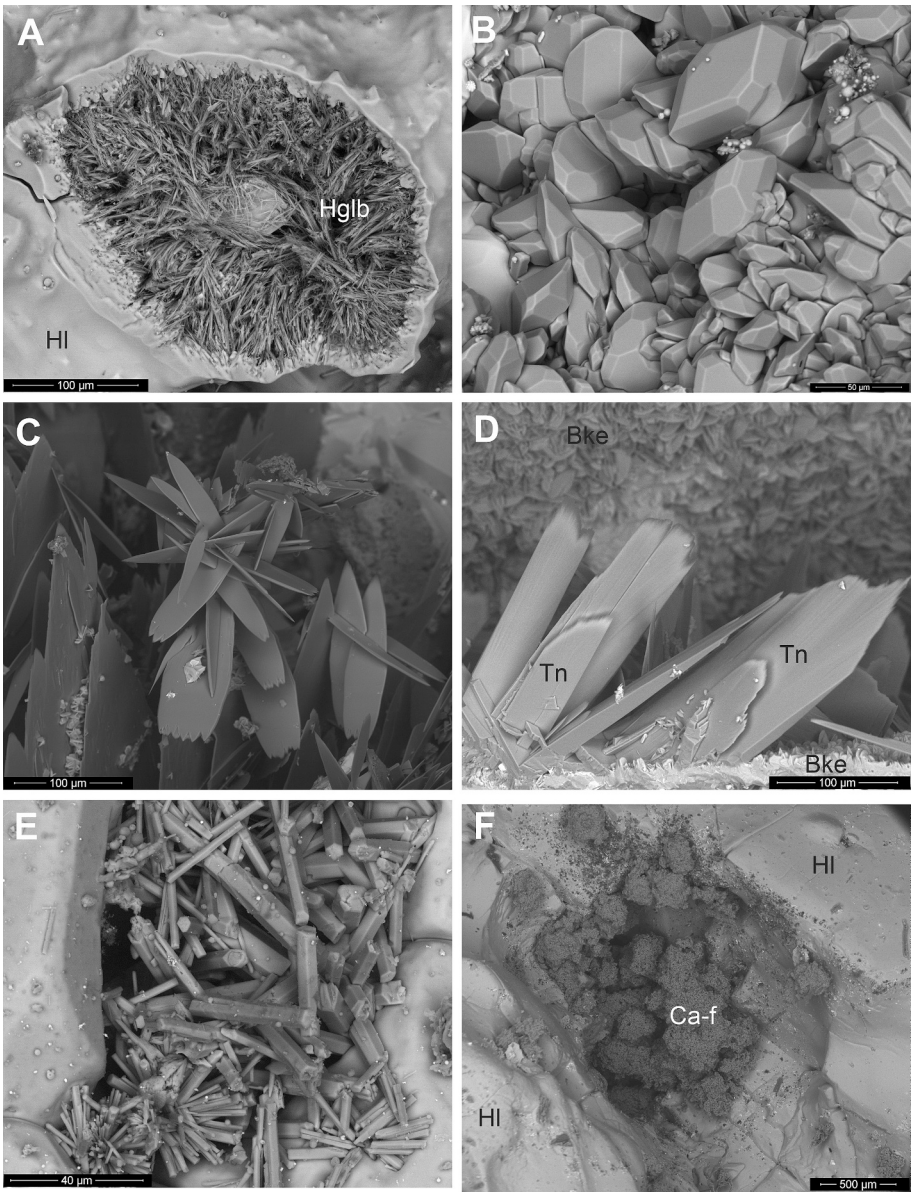

Fig. 5. Back-scattered electron images of group III and IV halite and sulfate stalactite minerals. A – acicular hydroglauberite (Hglb) surrounded by halite (Hl); B – tabular thénardite; C – thin lamellar thermonatrite aggregate; D – trona blades (Tn) inside cavity filled by burkeyite (Bke); E – pseudohexagonal omongwaite crystals in the halite vug; F – aggregate of α-calcium formate (Ca-f) on halite (Hl). A–D: Lazy Mine, E: Suchá-Stonava Mine, F: Hlubina Mine.

CALCITE $CaCO_3$ – is a main component of a smooth, light gray to beige stalactite from the collections of the Ostrava Museum (Jeremenko Mine, sample M398). Verified by PXRD.

CARNALLITE $KMgCl_3{\cdot}6H_2O$ – is relatively common on the surfaces of halite straws, but always only in microscopic dimensions. It forms mostly subhedral tabular crystals there (Fig. 3e). It has only been verified by SEM-EDS.

EPSOMITE $MgSO_4{\cdot}7H_2O$ – forms a glassy white admixture of sulfate stalactites and crusts at the Lazy Mine. It dehydrates quickly.

GLAUBERITE $Na_2Ca(SO_4)_2$ – was detected as an impurity in a hydroglauberite-impregnated coal sample. It is formed by dehydration of hydroglauberite. It was verified both by SEM-EDS microanalysis and PXRD.

GYPSUM $CaSO_4{\cdot}2H_2O$ – is only accessory on salt stalactites. It forms on the surfaces of stalactites arising from waters with higher content of sulfate ions. There it forms scattered microscopic crystals of variable size. At the Lazy Mine, it was found together with hydroglauberite on the surface of the coal seam, under the crust of evaporites.

HALITE NaCl – is the principal component of halite stalactites and a minor component of carbonate and sulfate (Matýsek et al., 2014) stalactites. It is also the only evaporite mineral that has been reported from mines in the Czech part of the Upper Silesian Basin so far. It mainly forms relatively long and thin straws of white color. They are also commonly colored by iron oxides or oxyhydroxides to orange or by coal dust to gray to black. The straws tend to have signs of cubic crystal development, sometimes highly skeletal (Fig. 2a, b) on the surface and in the central channel. Abundant octahedral halite crystals (Fig. 3d) were noticed at ČSA Mine, Jindřich Shaft.

HEXAHYDRITE $MgSO_4{\cdot}6H_2O$ – forms an admixture in sulfate stalactites and crusts at the Lazy Mine. It was verified by SEM-EDS and powder X-ray diffraction.

KAINITE $KMg(SO_4)Cl{\cdot}3H_2O$ – was detected as a microscopic (SEM) component in the form of imperfectly developed crystals (Fig. 4b) on the surfaces of halite stalactites from the Lazy Mine. It was verified by SEM-EDS and PXRD.

KONYAITE $Na_2Mg(SO_4)_2{\cdot}5H_2O$ – was found in only one sample from

the Lazy Mine. It forms microscopic, flattened crystals (Fig. 4c) on the surface of a beige-colored stalactite. It was verified based on SEM-EDS microanalysis and powder X-ray diffraction.

KRÁLÍKITE $BaCl_2{\cdot}2H_2O$ – occurs on surfaces, less often in the central channels of halite stalactites, which were formed by evaporation of sulfate-free waters. It forms microscopic, thin tabular, usually imperfectly developed crystals (Fig. 6). It has been verified by SEM-EDS, SEM-WDS, and XPS methods. For the full description see Section 4.3.

The mineral was recognized in number of occurrences across the active mines in the Czech part of the Upper Silesian Basin. The best documented are: 1. Mining Plant I, ČSA Mine (Jan Karel), crosscut 0930; 2. Mining Plant I, ČSA Mine, crosscut 01202; 3. Mining Plant II, ČSM Mine, crosscut 5301, stationing 1450 m, tectonic zone E1; 4. Hlubina Mine, halite stalactites stored in a collection of Mineralogical-petrographical Department of the Moravian Museum in Brno (No. 885–892).

LEPIDOCROCITE $Fe^{3+}O(OH)$ – is, together with akaganeite (Fig. 3a, b), a component of the surfaces of orange-colored halite stalactites according to powder X-ray diffraction. It has been also verified by SEM-EDS.

MONOHYDROCALCITE $CaCO_3{\cdot}H_2O$ – is a minor component of smooth, light gray to beige calcite stalactite from the collections of the Ostrava Museum (coming from Jeremenko Mine, sample No. M398). Verified by PXRD, in association with minor halite.

PENTAHYDRITE $MgSO_4{\cdot}5H_2O$ – according to powder X-ray diffraction, it forms only a minor admixture in sulfate stalactites and crusts at the Lazy Mine.

STARKEYITE $MgSO_4{\cdot}4H_2O$ – is the main component of sulfate stalactites and crusts at the Lazy mine. These stalactites are dull white, powdery and disintegrate easily (Fig. 4b). It has been verified by SEM-EDS and powder X-ray diffraction.

SYLVITE KCl – was found only as scattered microscopic cuboocta-hedral crystals (Fig. 2e, f) on the surfaces of halite stalactites. Some sylvite contains significant amount of Br (Fig. 4d) and even I, passing into yet undescribed mineral with nominal composition KBr. It was verified by SEM-EDS.

TACHYHYDRITE $CaMg_2Cl_6{\cdot}12H_2O$ – is formed by the action of vacuum on salt stalactites during SEM-EDS analyses. According to powder X-ray diffraction analyses, tachyhydrite is the main component of nodules and hollow spherical formations (blebs) that are released from stalactites in vacuum. It must be, therefore, considered an anthropogenic/artificial phase.

THÉNARDITE Na_2SO_4 – is a significant component in some of the halite stalactites from the Lazy Mine, identified by powder X-ray diffraction. Thénardite was found on irregularly developed, short stalactites with rough surface. It also forms an admixture in other types of stalactites at the Lazy site. Its irregular, flat microscopic crystals (Fig. 5b) can be observed in SEM. It was verified by both SEM-EDS and PXRD.

TRONA $Na_3H(CO_3)_2{\cdot}2H_2O$ – was found in the cavities of stalactites from the Lazy Mine. The cavities are filled with a powdery, light beige mass. Trona forms irregular thin tabular crystals (Fig. 5d) in this mass. It was verified by PXRD and SEM-EDS.

4.2.2. *Tentatively identified phases*

HYDROGLAUBERITE $Na_{10}Ca_3(SO_4)_8{\cdot}6H_2O$ – was found in the reaction zone between the coal seams and the halite crust. The coal sample is heavily impregnated with a white fibrous mineral (Fig. 5a), which according to powder X-ray diffraction corresponds to hydroglauberite. Problem is that proper structure of hydroglauberite including its space group was not yet published. It was also verified by SEM-EDS microanalysis.

OMONGWAITE $Na_2Ca_5(SO_4)_6{\cdot}3H_2O$ – forms elongated needles with pseudohexagonal shape up to 50 μm long (Fig. 5e). They came from a museum halite sample from the Suchá–Stonava Mine, accompanied by magnesium sulfate and gypsum. It is the fourth reported occurrence of

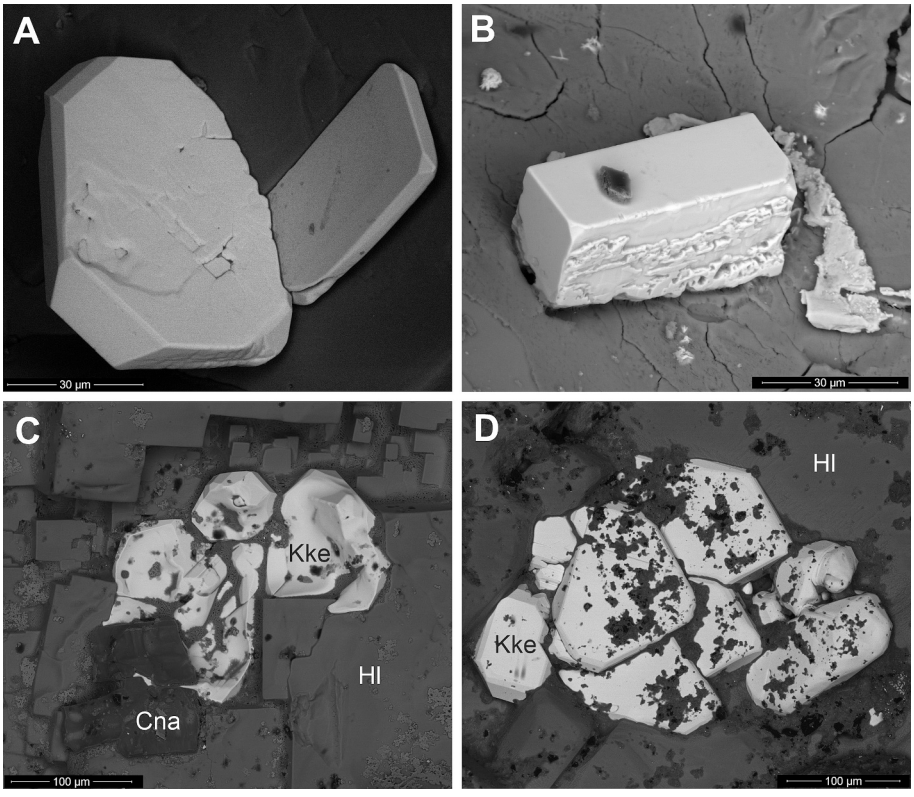

Fig. 6. Back-scattered electron images of králíkite from the ČSA Mine, Jan Karel Shaft. A – thin tabular with dominant (010) crystal faces; B – thick tabular králíkite crystal; C – králíkite (Kke) aggregate on halite (Hl) with younger carnallite (Cna); D – králíkite (Kke) aggregate on halite (Hl).

this mineral worldwide (Mees et al., 2008; Schorn et al., 2013; Sainz de Baranda Graf and Gaspar Sintes, 2023). It was detected only by SEM-EDS microanalyses.

SYNGENITE $K_2Ca(SO_4)_2{\cdot}H_2O$ – was detected in only one sample from the Lazy Mine. It forms microscopic tabular crystals on the surface of a beige-colored halite stalactite (Fig. 4f). It was detected only by SEM-EDS microanalyses.

THERMONATRITE $Na_2CO_3{\cdot}H_2O$ – was found in the cavities of halite stalactites from the Lazy Mine. The cavities are filled with a powdery, light beige mass. Thermonatrite, which forms microscopic, pointed crystals (Fig. 5c) in such mass, was interpreted only on the basis of SEM-EDS microanalyses.

4.2.3. Phases that do not correspond to known minerals

$SrCl_2{\cdot}2H_2O$? and $SrCl_2{\cdot}6H_2O$? – microscopic crystals, ≤ 20 μm in size (Fig. 3f), sometimes with well developed crystal faces, are present on halite stalactites from the ČSA Mine, Jan-Karel Shaft.

KBr and K(I,Br)? – on the surfaces of beige halite stalactites from the Lazy Mine, these phases form very thin coatings, sometimes with hints or fully developed cubic crystals with a size of up to 1–2 μm (Fig. 4e). Its detection is based on SEM-EDS microanalyses, which are only approximate due to the small grain sizes. However, the high content of Br and sometimes I in connection with K in the measured spots is indisputable.

4.3. New mineral králíkite, $BaCl_2{\cdot}2H_2O$ (IMA 2019–070a)

In 2019, a proposal of a new mineral $BaCl_2{\cdot}2H_2O$ labeled IMA 2019–070 was submitted to the International Mineralogical Association, Commission on New Minerals and Mineral Names (IMA-CNMMN). It was finally approved in July 2024 with the name králíkite.

The identity of králíkite with synthetic $BaCl_2{\cdot}2H_2O$ was proven by four independent methods, namely by 1) quantitative microchemical analysis using wavelength-dispersive X-ray spectroscopy (WDS), 2) powder X-ray diffraction (PXRD) and 3) synchrotron-based micro-X-ray diffraction (μ-XRD), and 4) X-ray photoelectron spectroscopy (XPS). Some of the properties of the new mineral could not be determined on natural samples because of the size and association. Many difficulties were encountered because králíkite grows on halite; both minerals are water-soluble, transparent to white. It is impossible to distinguish them by optical means and manufacture thin sections from the rough surface of the halite stalactites, capturing precisely the microscopic crystals of králíkite. Therefore, we refer in some properties to earlier data for synthetic material.

4.3.1. Occurrence

Králíkite forms single morphological type in the studied material. The mineral grows on the surface of halite stalactites. It occurs as thin to thick tabular crystals (Fig. 6a, b); max. 160 × 120 × 10 μm in size forming crystalline aggregates up to 350 μm in size (Fig. 6c, d).

The mineral was recognized in number of occurrences across the active mines in the Czech part of the Upper Silesian Basin (see Section 4.2.1). The best documented one, which is considered to be the type locality, is Mining Plant I, ČSA Mine (Jan Karel), crosscut 0930.

Associated minerals are halite, carnallite, sometimes akaganeite, lepidocrocite, on some samples also baryte, sylvite, and $SrCl_2{\cdot}nH_2O$ phases. The mineral is of the evaporite origin. It is subrecently formed in the environment of hypersaline brines (Pluta and Zuber, 1995; Matýsek et al., 2014) stored in the Miocene aquifer (Labus, 2005) entering both active and abandoned bituminous coal mine works.

4.3.2. Physical, chemical, and other properties

Both natural and synthetic $BaCl_2{\cdot}2H_2O$ are colourless (Winchell and Emmons, 1931), with the white streak recognized in synthetic material (Haidinger, 1824). Lustre is vitreous inclining to pearly in case of synthetic material, both natural and synthetic compounds are transparent (Haidinger, 1824). Fluorescence was not recognized either on synthetic (Hao et al., 2003) or natural phase.

Mohs hardness of synthetic material equals to 2.5 (Haidinger, 1824). There is no good cleavage (Winchell and Emmons, 1931), confirmed in this work by SEM investigation on synthetic $BaCl_2{\cdot}2H_2O$. Tenacity was recognized as brittle - sectile and fracture as conchoidal on synthetic material (Haidinger, 1824).

Published measured density for the synthetic material is 3.097 $g{\cdot}cm^{-3}$ (Lide, 2007). Calculated density is 3.103 $g{\cdot}cm^{-3}$ for the unit-cell given by Padmanabhan et al. (1978), 3.109 $g{\cdot}cm^{-3}$ for the unit-cell given by Bochkova et al. (1980).

It is optically biaxial (+): with values $\alpha = 1.635$, $\beta = 1.646$, $\gamma = 1.660$, respectively $\alpha = 1.6295(6)$, $\beta = 1.64191(10)$, $\gamma = 1.65829(10)$ according to Winchell and Emmons (1931) and Wulff and Heigl (1931), both for for sodium light with 589 nm.

Birefringence value 0.025 for sodium light (589 nm) was published by Winchell and Emmons (1931), while Wulff and Heigl (1931) got slightly different value for the same light wavelenght. Measured 2 V angle equals to 84° 50′ at ca. 625–750 nm and 83° 46′ at 589 nm (Winchell and Emmons, 1931). The optic plane is 010, Z ^ c = 8° (Winchell and Emmons, 1931). Information about light dispersion and pleochroism is not available.

From the collected high resolution Ba3d5 and Cl2p XPS spectra on both the natural specimens and a synthetic analogue, we proved that there are identical bonding schemes in both structures (see overlaid spectra on Electronic Supplementary Material Figs. S1 and S2). The Ba3d5 spectral band at 781 eV is close to previously published value of 781.6 eV for $BaCl_2{\cdot}2H_2O$ (Seyama and Soma, 1984), whereas Cl2p spectral band at 199.5 eV is close to values typical for $CaCl_2$ and other alkaline earth metal a metal chlorides. Therefore, both studied phases could be considered as mutual analogues.

Králíkite is soluble in water and alcohol, and potentially dangerous to humans due to its release of highly toxic Ba^{2+} ions.

4.3.3. Chemical composition

Analytical data for králíkite (average of 8 spot analyses) are given in Table 2. On the basis of (Cl + Br) = 2 atoms per formula unit (apfu), the empirical chemical formula is $(Ba_{0.85}Ca_{0.10}Na_{0.03}Sr_{0.02}Fe_{0.01})_{\Sigma 1.02}(Cl_{1.99}Br_{0.01})_{\Sigma 2.00}{\bullet}2H_2O$ (Table 3).

The simplified formula is $(Ba,Ca)Cl_2{\cdot}2H_2O$. The ideal formula is $BaCl_2{\cdot}2H_2O$, which requires Ba 56.22, Cl 29.03, H_2O 14.75, total 100 wt %. The theoretical water content is 14.75%, the molecular weight is 244.266 $g{\cdot}mol^{-1}$. The water content has not been determined directly due to the size of the natural aggregates. The mineral dehydrates easily in the vacuum of the electron microprobe.

4.3.4. Crystal structure and data

Two independent methods, micro-X-ray diffraction (μ-XRD) and powder X-ray diffraction (PXRD), clearly proved structure of investigated natural králíkite and its identity with the synthetic $BaCl_2{\cdot}2H_2O$. Unit cell parameters are given in Table 4, while the complete X-ray diffraction data and given in Electronic Supplementary Material

Table 2
Chemical data (in wt%) for králíkite. H_2O* - calculated based on the ideal content of 2 H_2O in the formula.

Constituent	Mean	Range (n = 8)	Stand. Dev. (σ)
Ba	51.63	47.15–57.05	3.68
Na	0.32	0.15–0.68	0.17
K	0.06	0.02–0.16	0.04
Ca	1.83	1.02–2.98	0.62
Sr	0.74	0.63–0.82	0.08
Fe	0.19	0.00–0.44	0.13
Cl	31.11	29.06–33.32	1.20
Br	0.22	0.00–0.35	0.10
H_2O*	14.75		
Total	101.96	97.36–105.56	3.00

Table 3
Chemical composition of králíkite based on the WDS microanalyses (wt%) and calculation of its empirical formula coefficients based on the total of 2 anions. H_2O* - calculated based on the ideal content of 2 H_2O in the formula.

	Average	1	2	3	4	5	6	7	8
Ba	51.62	54.76	57.05	56.21	49.83	51.72	47.61	47.15	48.68
Ca	1.83	1.65	1.02	1.44	2.35	1.11	2.21	2.98	1.89
Sr	0.74	0.65	0.63	0.63	0.82	0.78	0.82	0.81	0.79
Na	0.32	0.25	0.24	0.15	0.68	0.25	0.38	0.16	0.45
K	0.06	0.16	0.06	0.04	0.04	0.02	0.05	0.04	0.08
Fe	0.19	0.13	0.00	0.10	0.12	0.25	0.23	0.28	0.44
Cl	31.11	30.72	30.87	30.98	32.27	29.06	30.25	33.32	31.42
Br	0.22	0.28	0.00	0.28	0.23	0.18	0.35	0.24	0.17
H_2O*	15.86	15.67	15.68	15.80	16.45	14.81	15.45	16.98	16.01
Total	101.96	104.28	105.55	105.62	102.79	98.19	97.36	101.95	99.93
Structural formulae (apfu)									
Ba^{2+}	0.854	0.917	0.954	0.933	0.795	0.916	0.809	0.728	0.798
Ca^{2+}	0.104	0.095	0.058	0.082	0.128	0.067	0.129	0.158	0.106
Sr^{2+}	0.019	0.017	0.017	0.016	0.020	0.022	0.022	0.020	0.020
Na^{+}	0.032	0.024	0.024	0.015	0.065	0.026	0.039	0.015	0.044
K^{+}	0.004	0.010	0.004	0.003	0.002	0.001	0.003	0.002	0.005
Fe^{3+}	0.008	0.005	0.000	0.004	0.005	0.011	0.010	0.011	0.018
Σ	1.020	1.068	1.057	1.052	1.015	1.044	1.011	0.933	0.991
Cl^{-}	1.994	1.992	2.000	1.992	1.994	1.994	1.990	1.994	1.995
Br^{-}	0.006	0.008	0.000	0.008	0.006	0.006	0.010	0.006	0.005
Σ	2.000	2.000	2.000	2.000	2.000	2.000	2.000	2.000	2.000
H_2O*	2.000	2.000	2.000	2.000	2.000	2.000	2.000	2.000	2.000

Table 4
Comparison of selected crystallographic parameters for králíkite type material and synthetic $BaCl_2{\cdot}2H_2O$ phase. Note: Rwp for PXRD is 0.0622.

Material	Natural type material	Natural type material	Synthetic	Synthetic
Source	this study	this study	Padmanabhan et al. (1978)	Bochkova et al. (1980)
Method	μ-XRD	PXRD	s-XRD	s-XRD
Used equipment	synchrotron radiation source ANKA, 14 keV wavelength λ = 0.886 Å	diffractometer Bruker-AXS D8 Advance, CuKα radiation, wavelength λ = 1.5406 Å	CuKα radiation, wavelength λ = 1.5406 Å	diffractometer DRON-1,5, MoKα radiation
Crystal system	monoclinic	monoclinic	monoclinic	monoclinic
Space group	$P2_1/n$	$P2_1/n$	$P2_1/n$	$P2_1/c$
a (Å)	6.7424(43)	6.7225(8)	6.7215(2)	6.717(5)
b (Å)	10.9258(64)	10.906(1)	10.9080(3)	10.900(6)
c (Å)	7.1326(51)	7.1301(8)	7.1316(2)	9.696(6)
β (°)	90.943(48)	91.101(6)	91.173(5)	132.7(1)
V (Å^3)	525.36(59)	522.64(10)	522.28	521.713
Z	4	4	4	not given

Tables S23, S24 and Figs. S3 to S5.

A full description of the crystal structure including atomic positions and displacement parameters is given for the synthetic phase by Padmanabhan et al., 1978. The structure is composed of Ba^{2+}-centered polyhedra, with Ba^{2+} being coordinated by five Cl^{-} ions and four H_2O molecules (Padmanabhan et al. (1978) proposed 4Cl + 4H_2O coordination). Ba^{2+} polyhedra are sharing edges and form puckered 010 layers. The layers share edges and corners with adjacent corners to build a compact polyhedral network structure (Fig. 7).

Alternative structure analysis was published by Bochkova et al. (1980), which is based on single crystal X-ray diffraction. Both works provide an apparently topologically identical structure but differ in their description.

4.3.5. Name and type material

The proposed mineral is named in honour of Ing. Jiří Králík, CSc. (1933–1986) who graduated at Vysoká škola báňská in Ostrava (Czechoslovakia) and worked there under the supervision of prof. dr. Jaroslav Kokta, renowned Czechoslovak mineralogist. Ing. Králík spent most of his professional career at Department of Mineralogy, Petrography and Geochemistry at Vysoká škola báňská in Ostrava, but also held lectures at the Havana University in Cuba between 1964 and 1965.

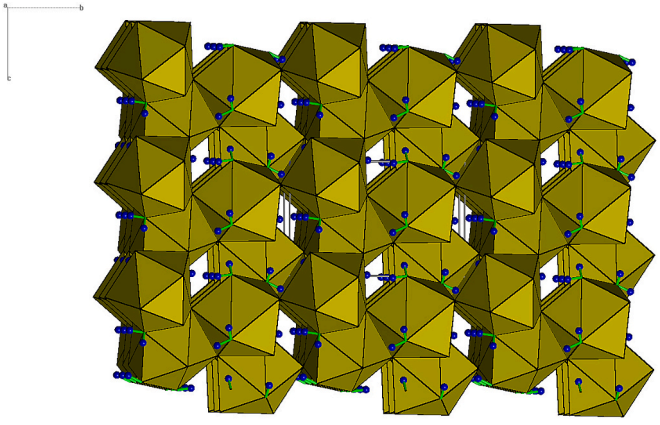

Fig. 7. Polyhedral representation of the crystal structure of králíkite projected onto (100) (after Padmanabhan et al., 1978). Brown polyhedra house the Ba^{2+} cations in nine-fold coordination with with O and Cl, blue circles correspond to H atoms. (For interpretation of the references to color in this figure legend, the reader is referred to the web version of this article.)

His research focused on clay minerals, mostly applied to the Upper Silesian Basin, and biomineralization. His scientific career was significantly hampered after 1968 by the political development in Czechoslovakia. We believe that he would have otherwise become a prominent world-renowned mineralogist in his field. He was also an excellent teacher, author or co-author of 1 scientific monograph, approximately 63 scientific articles, 44 proceeding papers, one geological map, 3 textbooks, and number of unpublished research reports (Kudělásek, 1987).

The holotype is deposited in the collection of the Department of Mineralogy and Petrology of the National Museum in Prague, Cirkusová 1740, Praha 9 (Czech Republic) under the catalogue number: P1P 19/2019. Part of the holotype is deposited in collection of the Mineralogical-petrological department of the Moravian Museum in Brno, Zelný trh 6, Brno (Czech Republic) under the catalogue number: A 11366. Another study material was deposited in the collection of the Geological museum of F. Pošepný at VŠB-Technical University of Ostrava.

5. Discussion

5.1. Genesis of CUSB evaporites

Evaporite minerals (both halides and sulfates) in the Czech part of the Upper Silesian Basin are similar to the common products of the marine water evaporation, as well as to some non-marine evaporites (e.g., Lindberg, 1946; Stewart, 1963; Casas et al., 1992; Jones and Renaut, 1996; Bąbel and Schreiber, 2014). However, there are major differences among the minerals described here and marine evaporites, such as: 1) chemical composition of brine, 2) constant chemical composition of the brines in time, and 3) generally low evaporation fraction.

The Upper Silesian hypersaline brines are highly mineralized and rich in Ba^{2+} (up to 1800 mg·l^{-1}), Sr^{2+} (up to 450 mg·l^{-1}), Br^{-} (up to 600 mg·l^{-1}), and I^{-} (up to 120 mg·l^{-1}). Examples of their chemical composition are given in Table 5 and publications of Pluta and Zuber (1995), Grmela (1997), Labus (2005), Dvorský et al. (2007), and Matýsek et al. (2014).

In our case, mineral precipitation is driven by succesive saturation of the solution at the constant temperature and ambient pressure in the underground spaces. Therefore, all minerals with solubility higher than that of halite are bound to the outer and inner surfaces of the halite stalactites. Neither phase transitions (dehydration reactions or metasomatic replacement) nor recrystallization were noticed.

The primary content of $(SO_4)^{2-}$ in brines is very low. The brines mix locally with acid mine drainage (AMD) waters generated by the pyrite weathering and strata of sulfate-bearing Variegated Beds (epigenetically altered segments and bodies of coal-bearing sediments) (Králík, 1980; Klika, 1999; Klika and Osovský, 1999). This mixing is documented by a continuous series beween halite precipitates (groups I and II of the halite stalactites in this study) and purely sulfate efflorescences as an AMD product in the USB mines described by Matýsek et al. (2014). An intermediate group are the halite stalactites of group III.

5.2. Comments on origin of some phases

Some of detected minerals call for a deeper discussion. The first of them is **tachyhydrite** that is not of natural origin and therefore does not comply with the definition of a mineral. Its origin is related to release of residual solutions from fluid microinclusions in halite under the vacuum conditions in SEM (chamber pressure 50 Pa). Under such conditions, micropores gradually appear on the observed surface and visibly enlarge until they almost foam (Fig. 8a). At the same time, bud-like formations emerge from the intercrystalline surfaces on the surface of the halite stalactites. These gradually solidify and, according to PXRD, contain predominantly tachyhydrite, while several weak diffraction lines belong to other unidentified phase(s). Almost all halite stalactites from groups 1 and 2 behave in this way.

Another case of possibly laboratory-grown phase in our research is **bischofite**. Its rare occurrence is probably linked with the hydration of carnallite during its storage, rather than to direct precipitation. However, such reaction is not a one-step process (Cheng et al., 2015; Hamze et al., 2024).

Uncertain is the origin of orthorhombic **α-Ca(HCOO)$_2$**. While tetragonal β-Ca(HCOO)$_2$ was recognized in nature and described under name formicaite (Chukanov et al., 1999), the orthorhombic polymorph does not have status of an approved mineral. It was described only from (Chukanov et al., 2021) sediments of the Alkali Lake (Oregon, U.S.), where it originates from anthropogenic chlorophenolic compounds that

Table 5
Chemical composition (mg·l^{-1}) of the selected mine waters from the places close to evaporite occurrences. For OKD, a.s. company prepared by Labtech Laboratories, accredited by Czech Accreditation Institute, now in the archive of authors. Note: b.d.l. - below detection limit, NA - not analysed.

Mine	Lazy		Dukla		ČSA – Jan Karel				
Sample No.	2947	3543	10,184	10,220	4001	7151	7152	12,833	14,384
pH	7.6	7.8	7.1	7.2	7.0	7.1	6.8	6.2	7.7
Mineralization	24,700	29,300	65,073	71,875	80,400	63,800	164,000	118,000	15,400
Anions									
Cl^{-}	14,800	18,000	29,340	45,990	50.300	40,000	102,000	76,100	8140
Br^{-}	78.9	88.3	369.1	231	231	184	474	310	33
I^{-}	4.9	2.5	18.7	10.2	b.d.l.	2.3	15.7	b.d.l.	b.d.l.
SO_4^{2-}	25.5	b.d.l.	820.3	513.4	b.d.l.	26.5	b.d.l.	b.d.l.	1190
HCO_3^{2-}	334	159	120.6	112.3	70.2	122	68.2	124	677
CO_3^{2-}	b.d.l.	b.d.l.	NA	NA	b.d.l.	b.d.l.	b.d.l.	b.d.l.	b.d.l.
Cations									
Na^{+}	8530	9960	28,800	20,700	22,500	17,700	44,300	29,200	4670
K^{+}	102	146	455	272	385	470	789	582	176
Ca^{2+}	534	609	3763	2926	4780	3900	11,800	7830	361
Mg^{2+}	261	315	1372	1101	1640	1260	3320	2430	129
Fe_{tot}	b.d.l.	b.d.l.	1.1	0.1	b.d.l.	0,1	b.d.l.	b.d.l.	0.10
Mn^{2+}	0.44	b.d.l.	0.01	1.8	0.28	1,68	7.89	5.76	0.85
Sr^{2+}	21.1	29.9	NA	NA	162	103	402	277	5.92
Ba^{2+}	7.6	37.3	NA	NA	330	32	556	761	0.19
Li^{+}	1.81	3.39	NA	NA	8.13	9.93	18.80	7.83	1.86
Al^{3+}	b.d.l.	b.d.l.	NA	NA	0.05	0.07	0.04	b.d.l.	b.d.l.
NH_4^{+}	4.89	b.d.l.	3	17.04	3.45	18.48	51.12	51.20	6.65

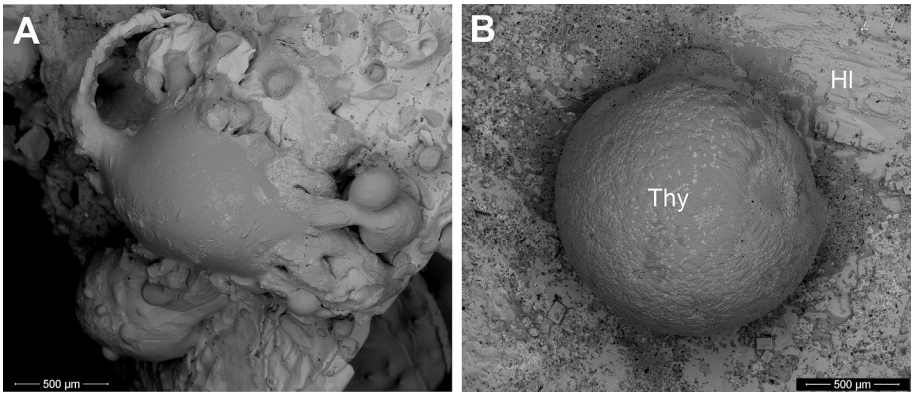

Fig. 8. Back-scattered electron images of tachydrite (Thy) blebs and spherical aggregates produced during electron microscope observation. A: Jan Karel Mine, B: ČSA Mine.

inhibit methanogenesis and enhance formate concentration. In case of our research, only one halite stalactite sample was found to contain abundant α-Ca(HCOO)$_2$ on its surface, accompanying králíkite. There is no clear evidence for either natural or artificial origin. Synthetic α-Ca(HCOO)$_2$ is used as an animal food preservant (summary in ESFA, 2014) and in construction industry for accelerating cement mortar and concrete (Geng et al., 2024). On the other hand, we see no reason to use this compound in underground coal mines in 1959, when the sample was collected, or later in the museum storage (no other samples stored in similar shelf were "contamined"). Obviously it is younger than králíkite, which is a proven product of natural brine evaporation.

5.3. Králíkite

Králíkite represents the first natural occurrence of barium chloride dihydrate, which is a common and long-known chemical. Its Chemical Abstract Service (CAS) number is CAS 10326-27-9. For the synthetic material, the infrared spectra are available for various spectral regions (Miller and Wilkins, 1952; Venkatesh and Neelakantan, 1966; Fukushima, 1971; Brink, 1972; Jain et al., 1976; Lutz et al., 1978). The near-infrared spectra were given by McCarthy and Walker (1990), far-infrared spectra were published by Fukushima and Kataiwa (1970). Raman spectra were published by Venkatesh and Neelakantan (1966), Jain et al. (1976), Lutz et al. (1978), and Kondyurin and Shkrabo (1998). The latter authors point out two crystallographically non-equivalent positions of H_2O in the structure. Polarized Raman spectrum of synthetic material was reported by Kanasaka et al. (1994).

Standard thermodynamic properties for the synthetic phase were published by Lide (2007). Thermogravimetric (TG) and differential thermal analysis (DTA) of synthetic $BaCl_2{\cdot}2H_2O$ was published by Paulik et al. (1968), Buzágh-Gere et al. (1972), and Wendlandt and Simmons (1972). Dehydration kinetics at 100 °C was described by Simmons and Wendlandt (1972), at 313–334 K by Osterheld and Bloom (1978), at stable temperatures ranging from 53.8 to 64.6 °C by Tanaka (1982). Differential scanning calorimetric analysis (DSC) was published by Guarini and Spinicci (1972).

The field of stability of various $BaCl_2$ hydrates is addressed by Fenstad and Fray (2006) in a binary system $BaCl_2$-H_2O phase diagram. In addition to $BaCl_2{\cdot}2H_2O$, there is also $BaCl_2{\cdot}H_2O$ and $BaCl_2{\cdot}0.5H_2O$ with limited stability. The only natural phase from this system is new mineral králíkite, while natural anhydrous $BaCl_2$ was described recently under name vegrandisite (Koděra et al., 2024).

5.4. Importance of the investigated evaporite mineralization

There are several reasons to consider and investigate the mineralization described in this contribution. The first reason is of mineralogical nature since our contribution greatly enhanced the diversity of minerals know from coal (Finkelman et al., 2019). Due to the unique chemistry of local brines, there is a potential for the description of few more new minerals in the future (e.g., Sr chlorides, Br analogue of sylvite). This study also points out that it is possible to study interesting geochemical processes in the environment of coal mines, mostly overlooked from the mineralogical perspective.

The second reason for interest in brines entering the coal matter is environmental. During the seam sampling, coal mine geologists avoid places with obvious evaporite mineralization, and the values for both chlorine and barium are highly variable across the basin. However, borehole data from the Polish part of the basin (whole coal, dry basis) given by Różkowska (1987) yielded 63–18,871 ppm Cl, which is far exceeding the maximum values for global medium- and high-rank coals (2300 ppm) or for global Late Carboniferous–Early Permian coals (max. 2290 ppm - all from Dai et al., 2025). For barium in Czech part of the Upper Silesian Basin, only the values from coal ash are available. They vary from 17 to 6170 ppm for various lithostratigraphical unit (Pešek et al., 2010).

Since the evaporite mineralization is highly soluble in water, there are significant environmental impacts related to the mine water discharge (e.g. Pluta, 2001; Bondaruk et al., 2015; Harat et al., 2015; Janson, 2024). These problems become even more prominent during the long-term flooding of the mines (in the Czech part, last one ceased production in February 2026). Since coal was used in local power plants, part of the chlorine, barium, and other elements was already released to the environment together with the gas emissions (e.g. Pluta and Plewa, 2018). Part of the evaporite mineralization was extracted with the coal tailing and stored in the heaps, which are also significant sources of uncontrolled release of elements like Cl, Br, and I into the environment (see Herzig et al., 1986; Matýsek and Jirásek, 2022).

6. Conclusions

The mine workings of the Czech part of the Upper Silesian Basin house an exceptionally rich evaporite assemblage. It contains a number of phases identified in the common seawater evaporites as well as some phases that are not typical for these chemical sediments. The main reason thereof is the specific chemical composition of the brines in the environment studied, with elevated content of Ba^{2+}, Sr^{2+}, Cl^-, Br^-, and I^-.

Evaporite mineralization itself represents an interesting scientific subject since the brine composition differs from the fluid usually encountered in near-surface environments, such as meteoric water or seawater-derived brine. However, the more important aspect of this mineralization is environmental. Due to the long history of coal mining in the Upper Silesian region, gas emissions from coal burning, discharge of mine waters, and storage of tailing on heaps, this mineralization has a potential of affecting the streams and soils on the surface. Because of

high solubility of most of the minerals described here, the load of dissolved and potentially toxic elements can fluctuate quickly and in a fashion that is not entirely predictable.

Future studies will be hampered by complicated access to suitable mining works and many of the sites will likely not be accessible soon. It is not only the approaching closure of coal mines. Another difficulty arises from the fact that these mineralizations occur in places with brine seepage and long-term evaporation, located mainly in abandoned mine workings with restricted ventilation as a prevention of coal self-ignition. Such sites are dangerous or impossible to reach and this situation will certainly only worsen with time. However, we can expect similar mineralizations in some bituminous coal basins at the Polish side of the Upper Silesian Basin, which share similar hydrogeological and hydrogeochemical situation.

Declaration of generative AI use

During the preparation of this work the authors used Google NotebookLM tool in order to prepare Graphical abstract. After using this tool, the authors reviewed and edited the content as needed and take full responsibility for the content of the published article.

CRediT authorship contribution statement

Dalibor Matýsek: Writing – review & editing, Writing – original draft, Visualization, Resources, Methodology, Investigation, Conceptualization. **Jakub Jirásek:** Writing – review & editing, Writing – original draft, Visualization, Supervision, Resources, Methodology, Investigation, Conceptualization. **Juraj Majzlan:** Writing – review & editing, Writing – original draft, Visualization, Resources, Methodology, Investigation. **Jan Filip:** Writing – review & editing, Investigation. **Michal Osovský:** Resources, Investigation. **Jörg Göttlicher:** Resources, Investigation.

Funding

The authors acknowledge the assistance provided by ERDF/ESF project TECHSCALE (grant number No. CZ.02.01.01/00/22_008/0004587).

Declaration of competing interest

Dalibor Matýsek: I have nothing to declare.
Jakub Jirásek: I have nothing to declare.
Juraj Majzlan: I have nothing to declare.
Jan Filip: I have nothing to declare.
Michal Osovský: I have nothing to declare.
Jörg Göttlicher: I have nothing to declare.

Acknowledgements

We are grateful to OKD company for granting access to the mines and permission to collect samples for our investigation. We would like to express our thanks to Ostrava Muzeum, Moravian Muzeum in Brno, and Prof. Pošepný's Geological Pavilion of the VŠB-Technical University of Ostrava for access to the museum samples. We are grateful to Radek Škoda from Masaryk University in Brno (Czechia) for the assistance with the electron microprobe analyses. The authors would like to thanks to two anonymous reviewers and editor-in-chief (Shifeng Dai) for the notes and guidance that helped to improve the quality of the manuscript.

Appendix A. Supplementary data

Supplementary data to this article can be found online at https://doi.org/10.1016/j.coal.2026.104990.

Data availability

Data will be made available on request.

References

Apostu, S.A., Panait, M., Vasile, V., 2022. The energy transition in Europe-a solution for net zero carbon? Environ. Sci. Pollut. Res. 29, 71358–71379. https://doi.org/10.1007/s11356-022-20730-z.

Aulický, Z., Iványi, K., Kafka, J., Kolek, M., Komínek, J., Kopecký, P., Machač, J., Staněk, V., Suček, P., Veselý, P., Vostatek, P., 2003. Rudné a uranové hornictví České republiky. Anagram, Ostrava (in Czech with Engish summary).

Bąbel, M., Schreiber, B.C., 2014. Geochemistry of evaporites and evolution of seawater. In: Holland, H.D., Turekian, K.K. (Eds.), Treatise on Geochemistry, 2nd edition 9. Elsevier, Oxford, pp. 483–560. https://doi.org/10.1016/B978-0-08-095975-7.00718-X.

Bartoňová, L., Raclavská, H., Čech, B., Kucbel, M., 2020. Behavior of Cd during coal combustion: an overview. Processes 8, 1237. https://doi.org/10.3390/pr8101237.

Bochkova, R.I., Grishin, I.A., Kuzmin, E.A., Belov, N.V., 1980. The refinement of the crystal structure of the barium chloride dihydrate $BaCl_2 \cdot 2H_2O$. Kristallografiya 25, 1064–1065 (in Russian).

Bondaruk, J., Janson, E., Wysocka, M., Chałupnik, S., 2015. Identification of hazards for water environment in the Upper Silesian coal basin caused by the discharge of salt mine water containing particularly harmful substances and radionuclides. J. Sustain. Min. 14, 179–187. https://doi.org/10.1016/0584-8539(72)80086-2.

Brink, G., 1972. Infrared studies of water in crystalline hydrates: $BaCl_2.2H_2O$. Spectrochim. Acta 28A, 1151–1155. https://doi.org/10.1016/0584-8539(72)80086-2.

Buzágh-Gere, É., Gál, A., Simon, J., 1972. Thermal investigation of the dehydratation of alkali earth chloride hydrates. In: Wiedemann, H.G. (Ed.), Thermal Analysis, Volume 2: Inorganic Chemistry. Birkhauser Verlag, Basel und Stuttgart, pp. 635–649.

Casas, E., Lowenstein, T.K., Spencer, R.J., Pengxi, Z., 1992. Carnallite mineralization in the nonmarine, Qaidam Basin, China; evidence for the early diagenetic origin of potash evaporites. J. Sediment. Res. 62, 881–898. https://doi.org/10.1306/D4267A05-2B26-11D7-8648000102C1865D.

Cheng, H., Ma, H., Hai, Q., Zhang, Z., Xu, L., Ran, G., 2015. Model for the decomposition of carnallite in aqueous solution. Int. J. Miner. Process. 139, 36–42. https://doi.org/10.1016/j.minpro.2015.04.007.

Chukanov, N.V., Malinko, S.V., Lisitsyn, A.E., Dubinchuk, V.T., Kuz'mina, O.V., Zadov, A.E., 1999. Formicaite $Ca(HCO_2)_2$, a new mineral. Zapiski Vseross. Mineral. Obshch. 128, 43–47 (in Russian).

Chukanov, N.V., Menor-Salvan, C., Gurzhiy, V.V., Izatulina, A.R., Pekov, I.V., Vigasina, M.F., Ksenofontov, D.A., Britvin, S.N., 2021. Biogenic orthorhombic α-calcium formate from sediments of Alkali Lake, Oregon, USA. Minerals 11, 448. https://doi.org/10.3390/min11050448.

Courbet, C., Wysocka, M., Martin, L., Chmielewska, I., Bonczyk, M., Michalik, B., Barker, E., Zebracki, M., Mangeret, A., 2016. Fate of radium in river and lake sediments impacted by coal mining sites in Silesia (Poland). In: Drebenstedt, C., Paul, M. (Eds.), Proceedings IMWA 2016 – Mining Meets Water – Conflicts and Solutions. TU Bergakademie Freiberg, Freiberg, Germany, pp. 1249–1253.

Dai, S., Seredin, V.V., Ward, C.R., Jiang, J., Hower, J.C., Song, X., Jiang, Y., Wang, X., Gornostaeva, T., Li, X., Liu, H., Zhao, L., Zhao, C., 2014. Composition and modes of occurrence of minerals and elements in coal combustion products derived from high-Ge coals. Int. J. Coal Geol. 121, 79–97. https://doi.org/10.1016/j.coal.2013.11.004.

Dai, S., Graham, I.T., Ward, C.R., 2016a. A review of anomalous rare earth elements and yttrium in coal. Int. J. Coal Geol. 159, 82–95. https://doi.org/10.1016/j.coal.2016.04.005.

Dai, S., Liu, J., Ward, C.R., Hower, J.C., French, D., Jia, S., Hood, M.M., Garrison, T.M., 2016b. Mineralogical and geochemical compositions of late Permian coals and host rocks from the Guxu Coalfield, Sichuan Province, China, with emphasis on enrichment of rare metals. Int. J. Coal Geol. 166, 71–95. https://doi.org/10.1016/j.coal.2015.12.004.

Dai, S., Hower, J.C., Finkelman, R.B., Ketris, M.P., Yudovich, Y.E., Zhang, Y., Liu, J., Zhao, C., Xu, N., Graham, I.T., French, D., Liu, Y., Yan, R., Zhao, Z., 2025. Abundances of elements in global coals. Int. J. Coal Geol. 311, 104899. https://doi.org/10.1016/j.coal.2025.104899.

Dedovets, I.G., 2025. Extracting germanium from Donetsk Basin coal. Coke Chem. 68, 407–410. https://doi.org/10.3103/S1068364X25600629.

Dopita, M., Kumpera, O., 1993. Geology of the Ostrava-Karviná coalfield, Upper Silesian Basin, Czech Republic, and its influence on mining. Int. J. Coal Geol. 23, 291–321. https://doi.org/10.1016/0166-5162(93)90053-D.

Dopita, M., Aust, J., Brieda, J., Černý, I., Dvořák, P., Fialová, V., Foldyna, J., Grmela, A., Grygar, R., Hoch, I., Honěk, J., Kaštovský, V., Konečný, P., Kožušníková, A., Krejčí, B., Kumpera, O., Martinec, P., Merenda, M., Müller, K., Novotná, E., Ptáček, J., Purkyňová, E., Řehoř, F., Strakoš, Z., Tomis, L., Tomšík, J., Valterová, P., Vašíček, Z., Vencl, J., Žídková, S., 1997. Geology of the Czech Part of the Upper Silesian Basin. Ministerstvo životního prostředí České republiky, Praha (in Czech with English abstract).

Dvorský, J., Malucha, P., Grmela, A., Rapantová, N., 2007. Ostravsko-karvinský detrit: spodnobádenská bazální klastika české části hornoslezské pánve. Montanex, Ostrava (in Czech with Engish summary).

Elavarasan, R.M., Pugazhendhi, R., Irfan, M., Mihet-Popa, L., Khan, I.A., Campana, P.E., 2022. State-of-the-art sustainable approaches for deeper decarbonization in Europe-

an endowment to climate neutral vision. Renew. Sust. Energ. Rev. 159, 112204. https://doi.org/10.1016/j.rser.2022.112204.
ESFA, 2014. Scientific opinion on the safety and efficacy of calcium formate when used as a technological additive for all animal species. EFSA J. 12, 3898. https://doi.org/10.2903/j.efsa.2014.3898.
Fenstad, J., Fray, D.J., 2006. The binary diagram water + barium chloride. C. R. Chim. 9, 1235–1242. https://doi.org/10.1016/j.crci.2006.02.004.
Filipović, S., Lior, N., Radovanović, M., 2022. The green deal – just transition and sustainable development goals *Nexus*. Renew. Sust. Energ. Rev. 168, 112759. https://doi.org/10.1016/j.rser.2022.112759.
Finkelman, R.B., Dai, S., French, D., 2019. The importance of minerals in coal as the hosts of chemical elements: a review. Int. J. Coal Geol. 212, 103251. https://doi.org/10.1016/j.coal.2019.103251.
Fu, X., Wang, J., Tan, F., Feng, X., Zeng, S., 2013. Minerals and potentially hazardous trace elements in the late Triassic coals from the Qiangtang Basin, China. Int. J. Coal Geol. 116-117, 93–105. https://doi.org/10.1016/j.coal.2013.07.013.
Fukushima, K., 1971. Low frequency infrared absorption bands of water of crystallization at low temperatures. Bull. Chem. Soc. Jpn. 44, 372–374. https://doi.org/10.1246/bcsj.44.372.
Fukushima, K., Kataiwa, H., 1970. Far-infrared spectra and lattice vinbrations of barium chloride dihydrate. Bull. Chem. Soc. Jpn. 43, 690–697. https://doi.org/10.1246/bcsj.43.690.
Geng, C., Chen, H., Qu, Y., Hou, P., Li, Q., Cheng, X., 2024. The effect of calcium formate on the performance of supersulfated cement. Ceramics-Silikáty 68, 216–224. https://doi.org/10.13168/cs.2024.0021.
Grmela, A., 1997. Hydrogeological conditions. In: Dopita, M. (Ed.), Geology of the Czech Part of the Upper Silesian Basin. Ministerstvo životního prostředí České republiky, Praha, pp. 198–204 (in Czech with English abstract).
Grobe, M., Machel, H.G., 2002. Saline groundwater in the Münsterland cretaceous Basin, Germany: clues to its origin and evolution. Mar. Pet. Geol. 19, 307–322. https://doi.org/10.1016/S0264-8172(02)00019-3.
Guarini, G.G., Spinicci, R., 1972. DSC study of the kinetics of the thermal dehydratation of $BaCl_2 \cdot 2H_2O$ and $BaCl_2 \cdot H_2O$. J. Therm. Anal. 4, 435–450. https://doi.org/10.1007/BF01913801.
Haidinger, W., 1824. On the crystalline forms and properties of several salts. Edinb. J. Sci. 1, 99–103.
Hammersley, A.P., 2016. FIT2D: a multi-purpose data reduction, analysis and visualization program. J. Appl. Crystallogr. 49, 646–652. https://doi.org/10.1107/S1600576716000455.
Hamze, R., Nevoigt, I., Sazama, U., Fröba, M., Steiger, M., 2024. Carnallite double salt for thermochemical heat storage. J. Energy Storage 86, 111404. https://doi.org/10.1016/j.est.2024.111404.
Hao, J., Lou, Z., Cocivera, M., 2003. In situ growth of blue-emitting thin films of cerium-doped barium chloride hydrate at low temperatures. Appl. Phys. Lett. 82, 1404–1406. https://doi.org/10.1063/1.1558891.
Harat, A., Rapantova, N., Grmela, A., Adamczyk, Z., 2015. Impact of mining activities in the Upper Silesian coal basin on surface water and possibilities of its reduction. J. Ecol. Eng. 16, 61–69. https://doi.org/10.12911/22998993/2806.
Havlena, V., 1982. The namurian deposits of the upper Silesian coal basin. Rozpr. Čs. Akad. Věd, Ř. mat. přír. věd 92, 1–79.
Herzig, J., Szczepańska, J., Witczak, S., Twardowska, I., 1986. Chlorides in the Carboniferous rocks of the Upper Silesian coal basin: environmental contamination and prognosis. Fuel 65, 1134–1141. https://doi.org/10.1063/1.1558891.
Hu, J., Chen, W.P., Zhao, Z.Q., Lu, R., Cui, M., Dai, W.J., Ma, W.M., Feng, X., Wan, X.M., Wang, N., 2022. Source tracing of potentially toxic elements in soils around a typical coking plant in an industrial area in northern China. Sci. Total Environ. 807, 151091. https://doi.org/10.1016/j.scitotenv.2021.151091.
Jain, Y.S., Kapoor, V.K., Bist, H.D., 1976. The infrared and Raman spectra of $BaCl_2 \cdot 2H_2O$ powder. Appl. Spectrosc. 30, 440–443. https://doi.org/10.1366/000370276774456976.
Janson, E., 2024. Multi-decadal impact of mine waters in Przemsza River Basin, Upper Silesian Coal Basin, Southern Poland. Water 16, 3147. https://doi.org/10.3390/w16213147.
Jaroš, Z., 1927. Nerostopisné drobnosti z Moravy. Příroda 20, 121–125 (in Czech).
Jedrzejek, F., Mendera, W., Szarlowicz, K., Heiss, N., Scherer, U.W., 2025. From coal ash to the nuclear fuel cycle: a new method of uraniumextraction with membranes. J. Environ. Manag. 392, 126644. https://doi.org/10.1016/j.jenvman.2025.126644.
Jirásek, J., Opluštil, S., Sivek, M., Schmitz, M.D., Abels, H.A., 2018. Astronomical forcing of Carboniferous paralic sedimentary cycles in the Upper Silesian Basin, Czech Republic (Serpukhovian, latest Mississippian): new radiometric ages afford an astronomical age model for European biozonations and substages. Earth Sci. Rev. 177, 715–741. https://doi.org/10.1016/j.earscirev.2017.12.005.
Jirásek, J., Matýsek, D., Alexa, P., Osovský, M., Uhlář, R., Sivek, M., 2020. High specific activity of radium isotopes in baryte from the Czech part of the Upper Silesian Basin – an example of spontaneous mine water treatment. Minerals 10, 103. https://doi.org/10.3390/min10020103.
Jones, B., Renaut, R.W., 1996. Skeletal crystals of calcite and trona from hot-spring deposits in Kenya and New Zealand. J. Sediment. Res. 66, 265–274. https://doi.org/10.1306/D4268315-2B26-11D7-8648000102C1865D.
Kalaitzidis, S., Siavalas, G., Skarpelis, N., Araujo, C.V., Christanis, K., 2010. Late Cretaceous coal overlying karstic bauxite deposits in the Parnassus-Ghiona Unit, Central Greece: coal characteristics and depositional environment. Int. J. Coal Geol. 81, 211–226. https://doi.org/10.1016/j.coal.2009.06.005.
Kalvoda, J., Bábek, O., Fatka, O., Leichmann, J., Melichar, R., Nehyba, S., Špaček, P., 2008. Brunovistulian terrane (Bohemian Massif, Central Europe) from late Proterozoic to late Paleozoic: a review. Int. J. Earth Sci. 97 (3), 497–518. https://doi.org/10.1007/s00531-007-0183-1.
Kanasaka, I., Matsuda, T., Niwa, Y., 1994. Raman intensity of lattice vibrations in $BaCl_2.2H_2O$. Many-body treatment. J. Raman Spectrosc. 25, 245–249. https://doi.org/10.1002/jrs.1250250308.
Karayiğit, A.I., Oskay, R.G., Christanis, K., Tunoğlu, C., Tuncer, A., Bulut, Y., 2015. Palaeoenvironmental reconstruction of the Çardak coal seam, SW Turkey. Int. J. Coal Geol. 139, 3–16. https://doi.org/10.1016/0166-5162(94)90010-8.
Klika, Z., 1999. Oxidative altered coal from the Upper Silesian Coal Basin. J. Czech Geol. Soc. 44, 335–342.
Klika, Z., Osovský, M., 1999. Thermally altered coal from Upper Silesian Coal Basin. J. Czech Geol. Soc. 44, 343–352.
Koděra, P., Majzlan, J., Pollok, K., Šimko, F., 2024. Vegrandisite, IMA 2023-045a. Eur. J. Mineral. 36, 602. https://doi.org/10.5194/ejm-36-599-2024.
Kondyurin, A., Shkrabo, D., 1998. Intermolecular vibrations of water molecules in the crystalline hydrates of $MCl_2.2H_2O$ (M=Cu, Fe, Mn, Ba, Co). J. Raman Spectrosc. 29, 607–611. https://doi.org/10.1002/(SICI)1097-4555(199807)29:7<607::AID-JRS276>3.0.CO;2-H.
Králík, J., 1980. Epigenetic oxidation in Red Beds from the Czechoslovak part of the Upper Silesian Coal Basin. In: Sborník vědeckých prací Vysoké školy báňské v Ostravě, řada hornicko-geologická, 26, pp. 107–123 (in Czech with English summary).
Kruťa, T., 1951. O nerostech z ostravsko-karvinského revíru. Přírodověd. Sbor. Ostrav. Kraje 12, 451–486 (in Czech).
Kruťa, T., 1973. Silesian Minerals and their Literatur. Moravské muzeum, Brno (in Czech with English summary).
Kučera, B., 1926. Doplňky k seznamu nerostů a nalezišť moravských za rok 1924 a 1925. Acta Mus. Morav. 24, 184–196 (in Czech).
Kudělásek, V., 1987. Ing. Jiří Králík, CSs., zemřel. Čas. Mineral. Geol. 32, 215–220 (in Czech).
Labus, K., 2005. Origin of groundwater mineralization in coarse-grained lower Badenian aquifer in the Czech part of the Upper Silesian Coal Basin. Geol. Q. 49, 75–82.
Larson, A.C., Von Dreele, R.B., 2004. General Structure Analysis System (GSAS). Los Alamos National Laboratory, New Mexico, USA.
Laurin, J., Kędzior, A., Naglik, B., Nadłonek, W., Opluštil, S., 2024. Eccentricity control on fluvial sedimentation in the tropics during the Middle-Late Pennsylvanian icehouse (~306-314 Ma, Upper Silesian Basin). Palaeogeogr. Palaeoclimatol. Palaeoecol. 654, 112420. https://doi.org/10.1016/j.palaeo.2024.112420.
Lide, D.R. (Ed.), 2007. CRC Handbook of Chemistry and Physics, 88th edition. Taylor & Francis Group, Boca Raton, Florida.
Lindberg, M.L., 1946. Occurrence of bromine in carnallite and sylvite from Utah and New Mexico. Am. Mineral. 31, 486–494.
Lutz, H.D., Pobitschka, W., Frischemeier, B., Becker, R.A., 1978. Lattice vibration spectra. XX. Infrared and Raman spectra of $BaCl_2.2H_2O$ and $BaCl_2.2D_2O$. Appl. Spectrosc. 32, 541–547. https://doi.org/10.1366/0003702787743308.
Malon, A., Tymiński, M., 2025. Węgle kamienne. In: Szuflicki, M., Malon, A., Tymiński, M. (Eds.), Bilans zasobów złóż w Polsce wg stanu na 31 XII 2024 r, 148. Panstw. Inst. Geol., Warszawa, pp. 42–52 (in Polish).
Maštalíř, V., 1926–1928. Recentní nerosty z karvinských dolů. Sbor. Přírod. Spol. Mor. Ostrava 14, 183–190 (in Czech).
Matýsek, D., Jirásek, J., 2022. Mineralogy of the coal waste dumps from the Czech part of the Upper Silesian Basin: Emphasized role of halides for element mobility. Int. J. Coal Geol. 264, 104138. https://doi.org/10.1016/j.coal.2022.104138.
Matýsek, D., Jirásek, J., Osovský, M., Skupien, P., 2014. Minerals formed by the weathering of sulfides in mines of the Czech part of the Upper Silesian Basin. Mineral. Mag. 78, 1265–1286. https://doi.org/10.1180/minmag.2014.078.5.12.
McCarthy, P.J., Walker, I.M., 1990. Single-crystal polarized spectra in the near-infrared region: a local mode analysis of the spectra of $BaCl_2{\cdot}2H_2O$. Inorg. Chem. 29, 820–824. https://doi.org/10.1139/v96-028.
Mees, F., Hatert, F., Rowe, R., 2008. Omongwaite, $Na_2Ca_5(SO_4)_6.3H_2O$, a new mineral from recent salt lake deposits, Namibia. Mineral. Mag. 72, 1307–1318. https://doi.org/10.1180/minmag.2008.072.6.1307.
Miller, F.A., Wilkins, C.H., 1952. Infrared spectra and characteristic frequencies of inorganic ions. Anal. Chem. 24, 1253–1294. https://doi.org/10.1021/ac60068a007.
Opluštil, S., Laurin, J., Hýlová, L., Jirásek, J., Schmitz, M., Sivek, M., 2022. Coal-bearing fluvial cycles of the late Paleozoic tropics; astronomical control on sediment supply constrained by high-precision radioisotopic ages, Upper Silesian Basin. Earth Sci. Rev. 228, 103998. https://doi.org/10.1016/j.earscirev.2022.103998.
Oskay, R.G., Christanis, K., Inaner, H., Salman, M., Taka, M., 2016. Palaeoenvironmental reconstruction of the eastern part of the Karapınar-Ayrancı coal deposit (Central Turkey). Int. J. Coal Geol. 163, 100–111. https://doi.org/10.1016/j.coal.2016.06.022.
Osterheld, R.K., Bloom, P.R., 1978. Dehydratation kinetics for barium chloride dihydrate single crystals. J. Phys. Chem. 82, 1591–1596. https://doi.org/10.1021/j100503a004.
Padmanabhan, V.M., Busing, W.R., Levy, H.A., 1978. Barium chloride dihydrate by neutron diffraction. Acta Crystallogr. B 34, 2290–2292. https://doi.org/10.1107/S056774087800792X.
Paulik, F., Paulik, J., Erdey, L., 1968. Combined thermo-dilatometric and derivatographic examination of hydrargillite and barium chloride dihydrate. Anal. Chim. Acta 41, 170–172. https://doi.org/10.1016/S0003-2670(01)80377-9.
Pešek, J., Sýkorová, I., Jelínek, E., Michna, O., Forstová, J., Martínek, K., Vašíček, M., Havelcová, M., 2010. Major and minor elements in the hard coal from the Czech Upper Silesian Paleozoic Basins. In: Czech Geological Survey Spec. Pap. Czech Geological Survey, Prague, p. 20.

Pluta, I., 2001. Barium and radium discharged from coal mines in the Upper Silesia, Poland. Environ. Earth Sci. 40, 345–348. https://doi.org/10.1007/s002540000175.
Pluta, I., Plewa, F., 2018. Pollution of coals of the Upper Silesian coal basin from the perspective of the European registers of the release and transfer of pollutants to air - the case of chlorine. In: Proceedings of the 4th Polish Mining Congress, IOP Conf. Series: Earth and Environmental Science, 174, p. 012011. https://doi.org/10.1088/1755-1315/174/1/012011.
Pluta, I., Zuber, A., 1995. Origin of brines in the Upper Silesian coal basin (Poland) inferred from stable isotope and chemical data. Appl. Geochem. 10, 447–460. https://doi.org/10.1016/0883-2927(95)00017-E.
Řanda, Z., Ulrych, J., Turek, K., Mihaljevič, M., Adamovič, J., Mizera, J., 2010. Radiobarites from the Cenozoic volcanic region of the Bohemian Massif: radiochemical study, history, and leas isotopic composition. J. Radioanal. Nucl. Chem. 283, 89–94. https://doi.org/10.1007/s10967-009-0095-6.
Różkowska, A., 1987. Content of chlorine in coals of the Upper Silesian coal basin. Kwartalnik Geol. 31, 57–68.
Sainz de Baranda Graf, B., Gaspar Sintes, I., 2023. Mineralogía de los filones '340' y '450' de Rodalquilar, Níjar, Almería, Andalucía. Paragénesis 4, 37–68 (in Spanish with English abstract).
Schorn, A., Neubauer, F., Bernroider, M., 2013. Polyhalite microfabrics in an Alpine evaporite mélange: Hallstatt, Eastern Alps. J. Struct. Geol. 46, 57–75. https://doi.org/10.1016/j.jsg.2012.10.006.
Seyama, H., Soma, M., 1984. X-ray photoelectron spectroscopic study of montmorillonite containing exchangeable divalent cations. J. Chem. Soc. Faraday Trans. 1 (80), 237–248. https://doi.org/10.1039/F19848000237.
Simmons, E.L., Wendlandt, W.W., 1972. Deaquation kinetics at the boiling point of water: $BaCl_2{\cdot}2H_2O$ and $BaBr_2{\cdot}2H_2O$. Thermochim. Acta 4, 291–294. https://doi.org/10.1016/0040-6031(72)87013-8.
Sivek, M., Jirásek, J., Kavina, P., Vojnarová, M., Kurková, T., Bašová, A., 2020. Divorce after hundreds years of marriage: prospects for coal mining in the Czech Republic with regard to the European Union. Energ Policy 142, 111524. https://doi.org/10.1016/j.enpol.2020.111524.
Starý, J., Mašek, D., Gabriel, Z., Němec, M., Hodková, T., Kavina, P., 2024. Mineral Commodity Summaries of the Czech Republic 2024. Czech Geological Survey, Prague.
Stewart, F.E., 1963. Marine evaporites. Data of geochemistry. In: U.S. Geological Survey Proffesional Paper 440-Y, Washington. https://doi.org/10.3133/pp440Y.
Sverdrup, H.U., Haraldsson, H.V., 2024. Assessing the long-term sustainability of germanium supply and price using the WORLD7 integrated assessment model. Biophys. Econ. Sustain. 9, 5. https://doi.org/10.1007/s41247-024-00121-3.
Tanaka, H., 1982. Kinetics of the thermal dehydratation stages of $BaCl_2{\cdot}2H_2O$ by means of TG at constant temperatures. Thermochim. Acta 52, 1–8. https://doi.org/10.1016/0040-6031(82)85178-2.
Thomas, L., 2013. Coal Geology, 2nd ed. Wiley-Blackwell, Chichester.
Tran, T.Q., Banning, A., Wisotzky, F., Wohnlich, S., 2020. Mine water hydrogeochemistry of abandoned coal mines in the outcropped Carboniferous formations, Ruhr Area, Germany. Environ. Earth Sci. 79, 84. https://doi.org/10.1016/S0264-8172(02)00019-3.
U.S. Energy Information Agency, 2011. Belfield Ashing Facility Site. Available at https://web.archive.org/web/20110812185141/https://www.eia.gov/cneaf/nuclear/page/umtra/belfield_title1.html.
Ulrych, J., Adamovič, J., Žák, K., Frána, J., Řanda, Z., Langrová, A., Skála, R., Chvátal, M., 2007. Cenozoic "radiobarite" occurrences in the Ohře (Eger) Rift, Bohemian Massif: mineralogical and geochemical revision. Chem. Erde Geochem. 67, 301–312. https://doi.org/10.1016/j.chemer.2005.05.003.
Vassilev, S.V., Yossifova, M.G., Vassileva, C.G., 1994. Mineralogy and geochemistry of Bobov Dol coals, Bulgaria. Int. J. Coal Geol. 26, 185–213. https://doi.org/10.1016/0166-5162(94)90010-8.
Vassilev, S.V., Vassileva, C.G., Baxter, D., Andersen, L.K., 2010a. Relationships between chemical and mineral composition of coal and their potential applications as genetic indicators. Part 1. Chemical characteristics. Geol. Balc. 39, 21–41. https://doi.org/10.52321/GeolBalc.39.3.21.
Vassilev, S.V., Vassileva, C.G., Baxter, D., Andersen, L.K., 2010b. Relationships between chemical and mineral composition of coal and their potential applications as genetic indicators. Part 2. Mineral classes, groups and species. Geol. Balc. 39, 43–67. https://doi.org/10.52321/GeolBalc.39.3.43.
Venkatesh, G.M., Neelakantan, P., 1966. Infra-red and Raman spectra of $BaCl_2{\cdot}2H_2O$ and $BaCl_2{\cdot}2D_2O$. Proc. Indian Acad. Sci. A 64, 36–43. https://doi.org/10.1007/BF03049329.
Wagner, N.J., Hlatshwayo, B., 2005. The occurrence of potentially hazardous trace elements in five Highveld coals, South Africa. Int. J. Coal Geol. 63, 228–246. https://doi.org/10.1016/j.coal.2005.02.014.
Wang, C.Y., Du, Y., Yan, B., Dong, Y.G., Zhao, Z.H., Shen, J.C., Guo, M.X., Zhang, Z.C., 2024. Composition, characteristics, and treatment technologies of condensable particulate matter present in flue gas emitted by coking plants in China. Sci. Rep. 14, 8522. https://doi.org/10.1038/s41598-024-59098-0.
Watanabé, T., Matsui, M., 1978. A redetermination of the crystal structure of α-calcium formate, α-strontium formate and barium formate by X-ray analyses. Acta Crystallogr. B 34, 2731–2736, 78. https://doi.org/10.1107/S0567740878009127.
Wei, Q., Song, W., 2020. Mineralogical and chemical characteristics of coal ashes from two high-sulfur coal-fired power plants in Wuhai, Inner Mongolia, China. Minerals 10, 323. https://doi.org/10.3390/min10040323.
Wei, Y., He, W., Qin, G., Fa, M., Cao, D., 2020. Lithium enrichment in the No. 2_1 coal of the Hebi No. 6 mine, Anhe coalfield, Henan Province, China. Minerals 10, 521. https://doi.org/10.3390/min10060521.
Wei, X., Xu, N., Chen, L., Chen, J., Li, J., 2024. Occurrence, mobility, and potential risk of uranium in an abandoned stone coal mine of Jiangxi Province, China. Environ. Earth Sci. 83, 531. https://doi.org/10.1007/s12665-024-11799-5.
Wendlandt, W.W., Simmons, E.L., 1972. A thermoanalytical investigation of the thermal deaquation of $BaCl_2{\cdot}2H_2O$ and $BaBr_2{\cdot}2H_2O$. Thermochim. Acta 3, 171–175. https://doi.org/10.1016/0040-6031(72)85026-3.
Winchell, A.N., Emmons, R.C., 1931. The Microscopic Characters of Artificial Inorganic Solid Substances or Artificial Minerals, 2nd edition. John Wiley & Sons, Inc., New York.
Wulff, P., Heigl, A., 1931. Refraktometrische Messungen an Kristallen. Z. Kristallogr. 77, 84–121. https://doi.org/10.1524/zkri.1931.77.1.84.
Wysocka, M., Chałupnik, S., Chmielewska, I., Janson, E., Radziejowski, W., Samolej, K., 2019. Natural radioactivity in Polish coal mines: an attempt to assess the trend of radium release into the environment. Mine Water Environ. 38, 581–589. https://doi.org/10.1007/s10230-019-00626-0.
Yossifova, M.G., Eskenazy, G.M., Valčeva, S.P., 2011. Petrology, mineralogy, and geochemistry of submarine coals and petrified forest in the Sozopol Bay, Bulgaria. Int. J. Coal Geol. 87, 212–225. https://doi.org/10.1016/j.coal.2011.06.013.
Zhao, L., Dai, S., Nechaev, V.P., Nechaeva, E.V., Graham, I.T., French, D., 2019. Enrichment origin of critical elements (Li and rare earth elements) and a Mo-U-Se-Re assemblage in Pennsylvanian anthracite from the Jincheng Coalfield, southeastern Qinshui Basin, northern China. Ore Geol. Rev. 115, 103184. https://doi.org/10.1016/j.oregeorev.2019.103184.